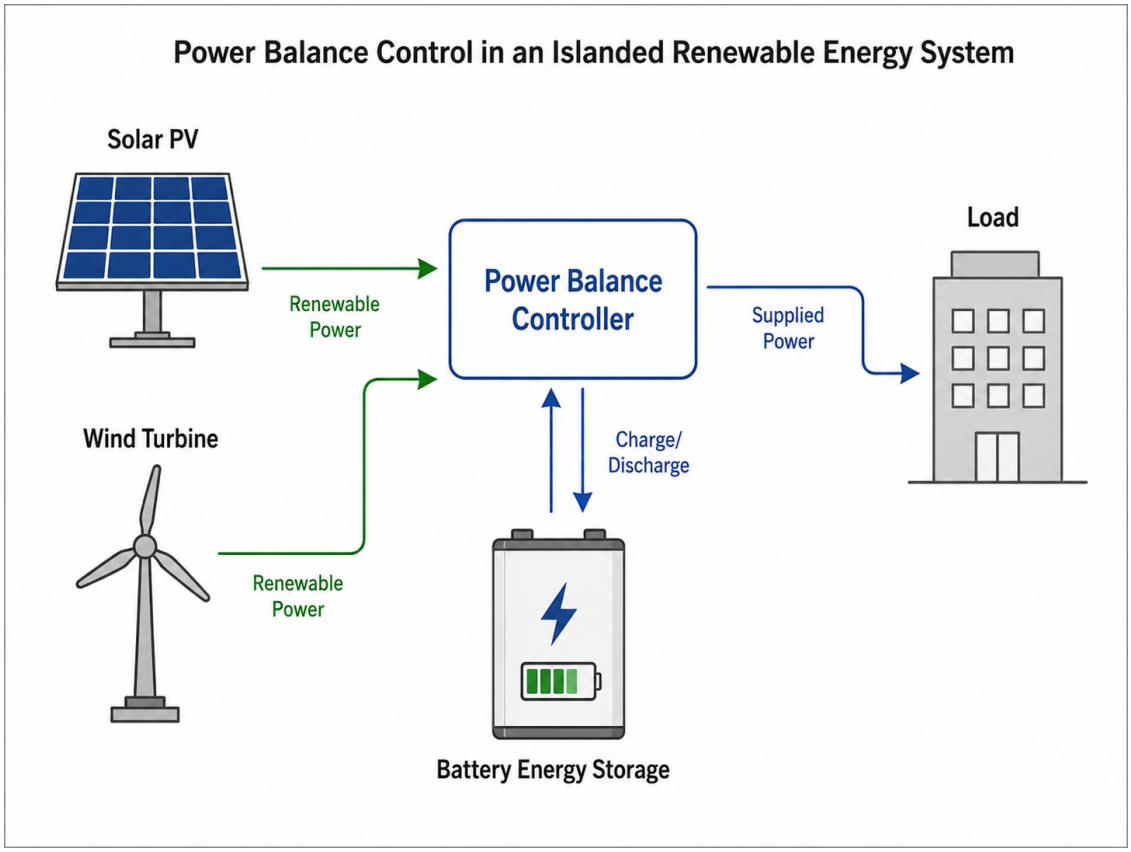
CHALMERS
UNIVERSITY OF TECHNOLOGY



Power Management Strategy for Islanded Operation Using Wind Power, Solar PV, and Battery Storage

Master's thesis in MPEPO

ABHIMANYU MOTTY, ALBI JINU

DEPARTMENT OF Electrical Engineering
CHALMERS UNIVERSITY OF TECHNOLOGY
Gothenburg, Sweden 2026
www.chalmers.se

Master's thesis 2026

Power Balance Control and Energy Management Analysis of an Islanded Wind–Solar–Battery System

Simulation-Based Analysis of Battery Charging and Discharging, Renewable Power Curtailment, Load Shedding, and Grid-Forming Converter Operation for Power Balance in an Islanded Wind–Solar–Battery System

Abhimanyu Motty, Albi Jinu



CHALMERS
UNIVERSITY OF TECHNOLOGY

Department of Electrical Engineering
Electrical Power Engineering
Chalmers University of Technology
Gothenburg, Sweden 2026

Power Balance Control and Energy Management Analysis of an Islanded Wind–Solar–Battery System
ABHIMANYU MOTTY, ALBI JINU

Supervisor: Ola Carlson,
Examiner: Ola Carlson, Electrical Engineering.

Master's Thesis 2026
Department of Electrical Engineering
Division of Electric Power Engineering
Unit of Power grids and components
Chalmers University of Technology
SE-412 96 Gothenburg
Telephone +46 31 772 1000

Typeset in LaTeX

Gothenburg, Sweden 2026

Power Balance Control and Energy Management Analysis of an Islanded Wind–Solar–Battery System
Simulation-Based Evaluation of Energy Management, Battery Charging and Discharging, Renewable Power Curtailment, and Load Shedding for Maintaining Power Balance in an Islanded Wind–Solar–Battery System Abhimanyu Motty, Albi jinu
Department of Electrical Engineering
Chalmers University of Technology

Abstract

As electricity demand grows and renewable energy becomes a larger part of the power system, maintaining a reliable supply during grid interruptions becomes increasingly important. Microgrids that combine wind power, solar photovoltaics and battery storage can supply local loads independently of the main grid. However, operating these systems in islanded mode requires careful coordination to balance changing generation and demand. This thesis investigates the islanded operation of a wind–solar–battery microgrid based on the Chalmers research wind turbine at Björkö, Sweden. A battery-connected grid-forming converter provides the voltage and frequency reference, allowing wind and solar generation to operate alongside it through grid-following converters. The main objective was to develop a power balance controller and evaluate its ability to work with the grid-forming converter during different operating conditions. The control logic was developed in MATLAB/Simulink to manage power surpluses and deficits while respecting battery state-of-charge and power limits. When renewable generation exceeds demand, the controller directs the surplus to the battery and curtails generation when necessary. When generation is insufficient, the battery supplies the shortfall, with load shedding used when the available power cannot meet demand. EMTP-RV simulations were then used to evaluate the interaction between the power balance controller and the grid-forming converter. The simulation results demonstrate how coordinated control of generation, storage and demand can support islanded operation within the system's operating limits. The work provides a basis for developing renewable microgrids that can maintain local electricity supply when disconnected from the main grid.

Keywords: Islanded Operation, Wind Power, Solar PV, Battery Storage, Energy Management System, Grid-Forming Converter.

Acknowledgements

We would like to express our sincere gratitude to our supervisor and examiner, Professor Ola Carlson, for his valuable guidance, encouragement, and support throughout our master's thesis. His knowledge, experience, and suggestions have helped us develop a better understanding of the subject and successfully complete this work. We are also thankful to Chalmers University of Technology for providing the necessary facilities, technical resources, and learning environment to carry out this research. The support and opportunities provided by the university have been valuable throughout our thesis work.

Abhimanyu Motty, Albi Jinu

Declaration of AI Use

During the preparation of this master's thesis, generative artificial intelligence tools, including ChatGPT (OpenAI), were used to assist with drafting and improving written content, reviewing technical concepts, LaTeX formatting, and troubleshooting code. These tools were mainly used to improve the clarity, structure, and presentation of the thesis. All AI-assisted content was reviewed and revised by the authors. The authors take full responsibility for the technical work, simulation results, analysis, and conclusions presented in this thesis.

List of Acronyms

Below is the list of acronyms used throughout this thesis, listed in alphabetical order.

AC	Alternating Current
AVM	Average Value Model
BESS	Battery Energy Storage System
DC	Direct Current
DER	Distributed Energy Resource
EMS	Energy Management System
EMTP	Electromagnetic Transients Program
ESS	Energy Storage System
FFR	Fast Frequency Response
GFL	Grid-Following
GFM	Grid-Forming
HAWT	Horizontal-Axis Wind Turbine
HVDC	High-Voltage Direct Current
IBESS	Integrated Battery Energy Storage System
MAE	Mean Absolute Error
MATLAB	Matrix Laboratory
MPP	Maximum Power Point
MPPT	Maximum Power Point Tracking
NMAE	Normalized Mean Absolute Error
NREL	National Renewable Energy Laboratory
NRMSE	Normalized Root Mean Square Error
PCC	Point of Common Coupling
PI	Proportional–Integral
PLL	Phase-Locked Loop
PQ	Active and Reactive Power
PV	Photovoltaic
RES	Renewable Energy Sources
RL	Resistance–Inductance
RMS	Root Mean Square
SOC	State of Charge
VSC	Voltage-Source Converter
WECS	Wind Energy Conversion System

Contents

Declaration of AI Use vii

List of Acronyms viii

Nomenclature ix

List of Figures xi

1 Introduction 1
- 1.1 Aim and Background . . . 1
- 1.2 Thesis scope . . . 3
- 1.3 Proposed Methodology . . . 3
  - 1.3.1 Literature and background study . . . 3
  - 1.3.2 System modelling in MatLab/Simulink and EMTP . . . 3
  - 1.3.3 Control strategy development . . . 4

2 Theoretical background investigation of previous island operation of wind turbines. 5

3 METHODS 9
- 3.1 WIND POWER . . . 9
  - 3.1.1 Basic Wind Turbine Theory . . . 9
  - 3.1.2 Wind Turbine Components and Their Functions . . . 11
  - 3.1.3 Simulink modeling of wind turbine . . . 11
    - 3.1.3.1 Model block 1- wind estimation . . . 11
    - 3.1.3.2 Model Block 2 – Power Estimation . . . 13
    - 3.1.3.3 Wind Turbine and Control System Implementation . 15
- 3.2 PV Model Development and Implementation . . . 16
- 3.3 Battery Energy Storage System Model . . . 19
- 3.4 Energy Management System for Wind–PV–Battery Power Balance . 21
- 3.5 Grid-Forming Converter Control Implementation . . . 23
  - 3.5.1 Active-Power Loop . . . 23
  - 3.5.2 Voltage-Reference Loop . . . 24
  - 3.5.3 Overall Control Structure . . . 25
  - 3.5.4 Overall Test Setup for GFM-Based Islanded Operation . . . 26
- 3.6 PLL Controller Implementation for the Grid-Following Converter . . 29
  - 3.6.1 Generation of the d-axis Current Reference . . . 30

3.6.2 PLL-Based Grid-Following Converter Test Setup 35

4 Results **39**
4.1 Battery Charging During Surplus Condition 39
4.2 Battery Discharging During Deficit Condition 41
4.3 Curtailment Operation During Full Battery Condition 42
4.4 Load Shedding During Empty Battery Condition 43
4.5 Result Discussion for the GFM-Based Islanded Case 44
4.6 Verification of Grid-Following Converter Synchronization 46
4.6.1 PCC Voltage Waveform 46
4.6.2 Verification of PLL Performance 47

5 Conclusion **49**

Bibliography **53**

A Appendix 1 **I**
A.1 MATLAB Code For the Islanded system I
A.2 MATLAB Code I
A.3 MATLAB Code used For the power balance controller XII

List of Figures

3.1 Wind Estimation Block. 12
3.2 Power estimation block. 14
3.3 Wind Turbine Control. 16
3.4 PV model implementation in Matlab. 17
3.5 Battery energy storage system model. 20
3.6 EMTP implementation of the grid-forming converter control structure. 25
3.7 Overall EMTPWorks test setup used to validate GFM-based islanded operation. 29
3.8 PLL control implementation in EMTP. 34
3.9 EMTPWorks test setup for the PLL-based grid-following converter. . 37

4.1 Power balance controller response during surplus. 40
4.2 Power balance controller response during deficit. 41
4.3 Curtailment response during surplus renewable generation with 100% battery SOC. 42
4.4 Load shedding response. 44
4.5 GFM behaviour at the PCC. 46
4.6 PCC voltage waveform during the PLL synchronization test with a stiff three-phase AC source. 47
4.7 PLL synchronization verification showing the q-axis voltage and estimated frequency during operation with a stiff AC source. 48

1
Introduction

This thesis examines the island operation of wind turbines along with solar power and battery storage with in a microgrid. The use of renewable energy is growing day by day and there are many promising opportunities in this field, but the main challenge is to ensure stable and reliable operation in isolated grids. The critical aspect of this work is to carry out an investigation to manage power balance by effciently using battery storage to maintain stability. The focus of this study is to develop Matlab/Simulink and EMTP models to improve interoperability between wind turbine, photovoltaic panel and battery. The intended outcome is to optimize the micro-gride performance and improve power distribution. This research builds on previous studies and includes practical testing using Chalmer's wind turbine and battery systems to validate the findings.

1.1 Aim and Background

In modern power system as part of energy sector shifting to sustainable electricity generation, the integration of renewable energy sources such as wind and solar is increasing year by year. The increasing adoption of renewable energy technologies is evident from the rapid growth in global installed capacity, which reached approximately 1291 GW of wind power and 2392 GW of solar power worldwide by the end of 2025[1], highlighting the expanding role of renewable resources in modern power systems[2]. This transition helps in minimizing the fossil fuel dependence and also thereby reducing greenhouse gas emission[2].However, penetrating Renewable energy sources (RES) into the existing power system is still a challenge. This is because these RES are inherently intermittent and highly dependent on environmental conditions. For instance, variation of wind speed and solar irradiance can rapidly change the output of the generators they are connected to which creates an unbalance between power generation and load demand[2]. Maintaining this balance is important in power system because deviation in generation and load demand affects voltage and frequency which can lead the system to go unstable[2]. To address these challenges and improve the reliability of renewable based power system, decentralized energy schemes known as microgrids have been widely proposed and studied[3]. A microgrid consists of a distributed generation units (DERs), local loads and sometimes a energy storage system which is operating within a defined electrical boundary[3].The advantage of this system is to operate either connected to a grid which is called grid connected mode or independently from the main grid which is called islanded operation [3].The islanded mode of the system allows the microgrid

to maintain power supply to the loads even during grid disturbance, thereby creating a reliable power system. In addition to good stability, microgrid also provides improved power quality, reduce transmission losses and also effective utilization of DERs[3]. Despite of these advantages, there are some technical challenges as the system no longer receives voltage and frequency support from the main grid. In conventional power system, large synchronous generator provides rotational inertia which helps in frequency stability, but such inertia is absent in microgrids as they are dominated by DERs and power electronic converters[3]. So they require appropriate control strategies and coordination among DERs to maintain stable voltage and frequency. Another important challenge is the mismatch between renewable power generation and the load demand[2]. When renewable energy generation become excess than the load demand, the excess power must be stored or curtailed to avoid instability[4]. Vice versa, when there is deficit generation in the microgrid additional power must be supplied to maintain the power balance[4]. Therefore Energy storage system(ESS) have became a critical component for this absorbing and suppling power conditions in microgrid thus by maintaining the microgrid stability. Various ESS technology is used in microgrids, including batteries, pumped hydro storage, flywheels, compressed air storage, and thermal energy storage systems[4]. Among these technologies, battery is widely used because of its fast response time, scalability and short term and long-term support for power balance capability[4]. Battery can improve microgrid stability by providing voltage and frequency support , decrease renewable power fluctuation by using interoperable control strategies. For example, microgrid studies have showed systems consisting of wind generators rated at approximately 7 MVA, suppling loads of about 2.21 MW, with additional photovoltaic generation contributing around 0.5 MW of power of the system[5]. In such systems battery storage system along with power electronic converters are typically used to maintain voltage levels around 6.6 kV on the microgrid bus while ensuring stable power delivery to connected loads[5]. To achieve this coordination, advance control strategies should be implemented in within the system. Primary control level which includes droop control which regulates voltage and frequency by adjusting active and reactive power and secondary control level helps in restoration of voltage and frequency to their nominal value and synchronize the microgrid with the main grid when reconnections occurs are the most commonly used control architectures[3]. Despite of numerous control strategies proposed to islanded microgrids, many existing approach still face limitations in terms of adaptability, communication requirement, and performance under dynamic conditions[3]. Therefore, further research is needed to develop improved control strategy that enable smooth integration of RES and ESS in islanded microgrid. Such research is important for supporting the transition towards sustainable power systems capable of operating with high levels of RES penetration. The aim of this thesis are to answer the following research questions:

- How should the wind turbine, solar PV, and battery be jointly controlled to achieve stable island operation under realistic load and generation variability?
- What control strategies minimize the battery cycling stress while maintaining system stability?
- What is the optimal battery size for different islanding scenarios ?

1.2 Thesis scope

- Theoretical background investigation of previous island operation of wind turbines
- Development of wind solar battery control strategy.
- Load profile definition
- Simulation based on MATLAB/Simulink and EMTP.
- Battery sizing optimization

.

1.3 Proposed Methodology

1.3.1 Literature and background study

In this phase, old thesis work and projects closely aligned with the proposal should be reviewed to develop the in depth understanding. The focus that should be kept in mind is to summarize the inverter-based control strategies. Analyse measurement data of Chalmers wind turbine power frequency response. Extract technical parameters: turbine power curve, PV sizing, battery and converter parameters, and load types.

1.3.2 System modelling in MatLab/Simulink and EMTP

In this phase the complete dynamic microgrid modelling will be conducted in Simulink and EMTP. The existing Chalmers wind turbine model will be used along with newly developed model for solar system and battery storage unit and the GFM. This will be connected to a common AC bus along with the varying load as proposed.[6] Component behaviour such as PV generation, battery SoC dynamics, and converter operation will be modelled to accurately represent expected real-world performance. This model will be the base for control design and the subsequent testing. The main objective is to verify that the system can maintain stable frequency and voltage despite variations in renewable generation and load demand. The simulations are expected to show power sharing between wind, PV and battery, battery charging and discharging behaviour (SOC evolution), curtailment during surplus generation, and the required battery size for reliable long-term operation. A scaled-up case 60 MW will also be analysed to assess performance at higher penetration levels. The EMTP simulations will focus on the electrical transient behaviour of the same system. These results will include detailed voltage and current waveforms, responses to sudden load changes and switching events, peak current stresses, and power quality indicators such as harmonic distortion. In summary, Simulink will validate control coordination and system-level stability, while EMTP will verify transient performance and electrical robustness of the converter-based system.

1.3.3 Control strategy development

This is the most crucial phase; a coordinated control strategy will be developed to ensure stable island operation. The power dispatch logic will prioritise renewable generation first, allowing wind and solar to produce up to their available resource level[6]. While battery absorbs excess power or supplies power during deficit[6]. When the battery approaches its limit protective actions like wind and PV curtailment and if necessary controlled load reduction will be implemented[6]. Frequency and voltage management will be achieved through the grid forming converter[8]. Reference set points for the GFM will be from that of the stand-alone grid. Battery output power will be adjusted based on the frequency deviation [5], while wind turbine operates with droop characteristics derived from prior experimental measures. This enables stable and responsive behaviour during unpredicted events.

2

Theoretical background investigation of previous island operation of wind turbines.

Islanded operation of wind turbine has become a crucial topic because modern power systems are expected to remain functional during outages, severe disturbances or intentional separation from the main grid, and our thesis places the Chalmers wind turbine, battery system and solar panel exactly in that context as a locals supply alternative for customer when grid support is unavailable. From a theoretical viewpoint, islanded operation of wind turbine can be understood through microgrid concept, where distributed energy resources (DERs), Energy storage system (ESS), and the loads are coordinated in such a way that it can provide voltage control, power sharing, and power balance without relying on the main grid[10]. The literature review make it clear that for a islanded system, at least one grid forming unit is required for establishing the voltage reference and for managing power balance, this also creates a electrical reference for other converter based units to follow.[10]. The difference between the gird forming and grid following behaviour is one of the most important theoretical idea behind previous islanded operation studies of wind system. Grid following converters (GFL) requires a voltage waveform from the grid for synchronization, whereas Grid forming converters (GFM) can create their own voltage and frequency reference, which is why GFM is extensively used for operations such as black-start and islanded operation with battery systems[11] Earlier work on islanded operation also shows that primary control can be set either through communication based coordination or through decentralized droop based control.[10]. Among this, droop based control was more common as it reduced communication requirement and also support independent operation of parallel converters[10]. At the same time conventional droop control has well known limitations such as line impedance mismatching which reduces accuracy in proper power sharing between the parallel inverters[10]. A more recent development in the literature is the use of virtual impedance together with enhanced droop control to reduce power sharing error caused by line impedance mismatching between parallel inverter paths to maintain more stable voltage and frequency under renewable source variability[12]. For wind-integrated systems this scheme is beneficial because wind fluctuations provides weak coordination which in turn affects the controller quality for providing stability and efficiency[12]. The same study also shows why simulation environments such as MATLAB/Simulink are valuable in this field, since they allow dynamic evaluation of voltage, frequency, and power-sharing behaviour before practical deployment[12].In

stand alone wind energy conversion system(WECS), the Converter cannot operate in the same way as it does when the turbine is connected to the main grid. The study by Asensio et al. shows that in a full converter WECS supplying an isolated load, the line side converter is used to establish voltage and frequency, while the generator side keeps the dc link voltage stable[13]. This means that the usual roles of the converters are effectively reversed compared with normal grid-connected operation[13]. An important factor of this arrangement is that the wind turbine can no longer simply provide maximum power point tracking (MPPT) and inject whatever power available from the wind ,instead the turbine has to operate in load following manner[13]. In other words, once the system is islanded, stable operation depends not only on harvesting wind energy, but also on continuously matching turbine output with load demand. The same study further explains that this balance can be achieved through pitch-based control[13]. When the load increases, the turbine must extract more power from the wind, and this is done by adjusting the pitch angle so that the mechanical input better matches the electrical demand[13]. However, pitch control acts more slowly than the converter, so during sudden changes the short term mismatch between load power and turbine power is temporarily absorbed through the turbines stored kinetic energy[13]. Another useful contribution of this control strategy is the inclusion of an inner current control loop within the voltage and frequency controller[13]. This improves protection during islanded operation because it helps regulate converter current and reduces the risk of converter overloading during disturbances or sudden load changes[13]. Further literature study on offshore wind turbines shows that islanded operation is not limited to supplying one load, But can involve supplying many loads in an island through coordinated control across a wind farm and its transmission system[14]. The author explains that during islanded operations, the offshore system must continue to maintain its voltage and frequency state while also keeping the HVDC link energized at its rated value[14]. At the same time the wind turbine are not expected to deliver full generated power to the external grid but only the active power require to cover the losses of the whole system[14].This same work shows the control responsibilities among the main converters in the system , where offshore AC grid voltage and frequency control is done by the front end converters of the wind turbine[14]. the voltage source control (VSC) is assigned with the task of maintaining the HVDC link voltage[14]. Although this study is based on an offshore wind farm with HVDC transmission, it is still relevant as general background because it highlights the central role of converter coordination in maintaining stable islanded operation The literature study based on integrated battery energy storage system (IBESS) brings battery into the picture. In this research the grid forming role is not only assigned to wind turbine but also to a battery supported converter installed at the point of common connection.[15]. In the IBESS study, this unit is used to energize the offshore grid, provide fast reactive support and also balance the power thus keeping the system stable[15]. The controller is explicitly grid forming and is based on power synchronization control for generating frequency and phase angle, together with voltage magnitude regulation and current limiting[15].Although this study is based on an offshore wind power plant, it is still relevant as general background for this thesis because it shows how a battery-supported converter can establish and maintain is-

landed operation, which is conceptually close to the separate grid-forming battery converter. Pagani et al further shows the battery-centered approach to islanded operation by showing that the grid connected BESS can operate together with a grid following wind turbine, allowing the battery to establish the island first while the wind turbine is synchronized afterwards[11]. The same study further shows that the battery initially handles the system energization and the active and reactive power supply , then the wind turbine periodically takes over the load and recharge the battery[11]. This is closely related to present thesis, which also includes a separate grid-forming battery converter in the system layout. Anant Narula's Chalmers PhD thesis provides further support for this battery centered understanding of grid forming operations in wind-based power system. Narula states that wind power plants are expected to provide ancillary services such inertia responses, frequency support etc. for this some form of energy storage system is required[16]. He further argues that adding a grid forming battery system at the point of common coupling is a further way to introduce grid forming behaviour.[16]. An important advantage of this addition is that there is no need of change in the internal control structure of the wind turbine[16].The study by Narula showed that it can improve the transient performance of the wind power plant and help it to operate well in weak grid condition[16]. For the present thesis, this is especially relevant because it creates a useful bridge between broader wind-power-plant theory and the smaller Chalmers islanded system. The 2024 study on Chalmers Research wind turbine was based on Islanded system where wind turbine could operate without connected to the main grid with support from PV cell and battery ESS. This study views islanded operation as a coordination problem between generation storage and demand.[6]. The literature states that for stable islanded operation we should maintain a periodic balance between the available renewable generation, the battery storage, and the load demand[6]. Because of wind and solar being naturally variable, the study shows the need for a intelligent control scheme which can respond to this sudden changes[6]. In this perspective controller becomes the main operating part of the system for maintaining stability by deciding which source or combination should be deployed for reliable power supply[6]. Some other functionality of this controller is battery management, load management thereby creating a overall power balance[6]. The study explains this control scheme through a set of operation condition. When wind power alone is enough, the controller allows the wind turbine to supply the full load, if there is any excess power that will be directed to battery for charging, and if the battery is also full the wind power will be curtailed[6]. when the wind power becomes lower, the system will move towards combined operating mode in which wind and solar together is used to meet the demand[6]. If wind and solar is deficit then battery is brought in to support the load along with the available power from wind and solar[6]. This makes the overall system flexible since the supply is not tied to one single source but can shift smoothly depending upon the operating conditions. In this literature the author presents battery as a active part of islanded system rather than being a passive reserve. The battery stores renewable energy when the generation is higher than demand and discharge when the renewable production falls below the load requirement[6]. The study also shows that battery size has a direct effect on reliability because larger battery can support the load for a

longer time periods of low generation and high demand[6]. At the same time, the study also depicts that a larger battery also needs more charging time and more input power which creates need for larger system[6]. Overall, this old literature is important because it shows that islanded wind-turbine operation should be understood as coordinated hybrid operation involving wind, solar, battery storage, and supervisory control rather than as the isolated behaviour of a wind turbine alone.

3
METHODS

3.1 WIND POWER

This chapter presents the theoretical background of wind power and its role in the islanded energy system considered in this thesis. The discussion begins with the basic concept of a wind turbine, including its main components and the process by which wind energy is converted into mechanical and electrical power. The key aerodynamic power equations are then introduced to explain how wind speed, rotor swept area, air density, tip speed ratio, and power coefficient influence the power extracted from the wind. In the proposed islanded system, which includes a wind turbine, solar PV, and battery storage, wind power is a central energy source because it provides the highest rated generation capacity among the two sources. For the Chalmers research wind turbine considered in this work, the rated power is approximately 30 kW

3.1.1 Basic Wind Turbine Theory

A wind turbine is an energy conversion device that capture the the kinetic energy from the moving air and converts it into mechanical torque at the turbine shaft[21]. In a wind energy conversion system, this mechanical power is then converted into electric power by using an electrical generator[22]. This electrical power can be used for supplying the local grid or can be stored using ESS (Energy storage system) for the providing grid support[22]. Among the various design profiles of the wind turbine the most common design profile used around the world is HAWTs (horizontal axis wind turbine). The HAWTs is like two or three blades (commonly three) mounted on a hub at the top of a tower[21]. Three blade HWATs are widely used because this arrangement gives a practical balance between aerodynamic performance, structural loading, rotational smoothness, and mechanical design complexity[19]. The energy available from a wind turbine depend mainly on wind speed, air density and area swept by the rotor blade[21]. The wind power from the wind passing through the rotor area can be mathematically represented as :

$$P_v = \frac{1}{2}\rho A v_w^3 \tag{3.1}$$

where P_v is the power available in the wind, ρ is the air density, A is the swept area of the rotor, and v_w is the wind speed[19].

For a circular rotor, the swept area is given by:

$$A = \pi r^2 \tag{3.2}$$

where A is the swept area of the rotor and r is the blade radius of the turbine.

The above equation shows the ideal power available from the wind turbine. The cubic relation between the wind speed and the wind power shows that even small variation in the wind speed can produce a large variation in the available wind power[18]. A wind turbine cannot convert all the kinetic energy into mechanical power because air must continue to flow through and behind the rotor[19]. The maximum theoretical fraction of wind power that can be extracted by an ideal wind turbine is defined by the Bertz limit, which is approximately around 59.3 %[22]. Therefore the practical wind turbine is represented including the power coefficient Cp, which describes the fraction of available wind captured by the rotor[19]. So the mechanical power equation of the wind turbine can be rewritten as:

$$P_m = \frac{1}{2}\rho A C_p(\lambda, \beta) v_w^3 \tag{3.3}$$

where P_m is the mechanical power extracted by the rotor, ρ is the air density, A is the swept area of the rotor, $C_p(\lambda, \beta)$ is the power coefficient, λ is the tip speed ratio, β is the blade pitch angle, and v_w is the wind speed[22].
The Cp is not constant as it depend upon the aerodynamics design of the turbine i.e. the tip speed ratio and the blade pitch angle. Here the tip speed ratio is the ratio between the blade tip speed and the incoming wind speed[20]. For a given turbine there is an optimum tip speed ratio at which the Cp reaches its maximum value[21]. When the turbine is operating near this optimum point, the rotor captures maximum possible mechanical power for the given wind condition[21].

The torque produced at the turbine shaft is related to the extracted mechanical power and rotor speed by:

$$T_m = \frac{P_m}{\Omega} \tag{3.4}$$

where T_m is the mechanical torque, P_m is the mechanical power extracted by the rotor, and Ω is the rotor angular speed[21]. In practical operation the turbine starts to produce useable power only when the wind speed exceeds the cut in speed and its output increases with wind speed until the rated power region is reached [22]. At higher wind speed to protect the mechanical and electrical system from excessive loading due to excess turbine power, limitation like pitch control is used [22]. Pitch control changes the blade angle to regulate the aerodynamic power capture from the wind, especially when the wind speed is above the rated operating region[22]. For an islanded wind–solar–battery system, these wind turbine characteristics are important because the wind power input is variable and must be coordinated with storage and other generation sources to maintain the balance between production and consumption.

3.1.2 Wind Turbine Components and Their Functions

A wind turbine is made up of mechanical, electrical and control components that work together to convert wind energy into electrical energy. The main parts of a typical wind turbine include rotor blades, hub, low-speed shaft, gearbox, high-speed shaft, generator, nacelle, tower and foundation[22]. The rotor blades are the part which captures the incoming wind and produce rotational motion[22]. The blades are then connected to the hub; the combination of blades and hub forms the rotor of the wind turbine [22]. The rotor then transfers the wind energy as mechanical rotational energy through the low-speed shaft[22]. Then the gearbox increases the low rotational speed of the rotor to a higher speed which is an input for the electrical generator and this higher speed is carried by a high-speed shaft[22]. The generator converts the rotating mechanical energy into electrical energy[21]. Components like the gearbox, shafts, generator, and control or electrical equipment are housed within nacelle which is located at the top of the tower [22]. Here, the tower functions as a support for the nacelle and also raise the rotor to a suitable height where the rotor can capture more wind[22]. The pitch system adjusts the blade pitch angle to control how much aerodynamic power is captured from the wind[22]. The yaw system turns the nacelle and rotor toward the wind direction so that the blades can face the incoming wind effectively[18]. In variable speed wind turbines, power electronic converters are used so that the generator can operate at variable speed, while the electrical output is converted into AC power with the required frequency.[22]. After this converter stage, a transformer is used to match or step up the voltage to the required AC grid or local bus voltage.

3.1.3 Simulink modeling of wind turbine

3.1.3.1 Model block 1- wind estimation

This block is used from estimating the wind speed experienced by the turbine, instead of directly using the measured wind speed from the nacelle sensor. The reason is that the measured wind speed can fluctuate faster than the actual turbine response. This happens because the wind sensor has much lower inertia when compared to the turbine rotor.[20]. Inputs to the wind estimation blocks are mechanical power P_{m}, blade-tip speed V_{tip}, and pitch angle β. The blade tip speed is calculated as:

$$V_{\mathrm{tip}} = \frac{2\pi \cdot \mathrm{N}}{60} R \tag{3.5}$$

In Equation 3.5, N represents the measured rotor speed from the rotor speed sensor in rpm, and R represents the rotor radius.

Inside the block the tip speed ratio is calculated by dividing the blade tip speed by the estimated wind speed to calculate the tip speed ratio.

$$\lambda = \frac{V_{\mathrm{tip}}}{v} \tag{3.6}$$

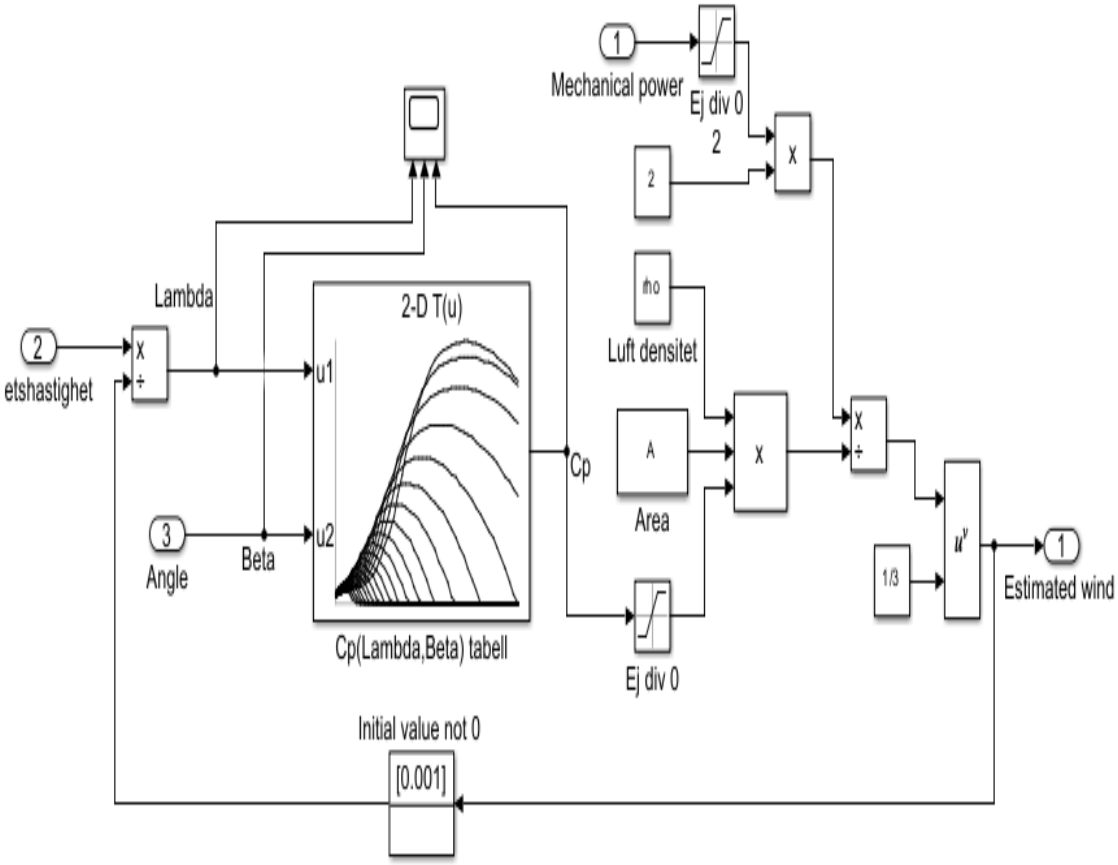


Figure 3.1: Wind Estimation Block.

Here the the estimated wind speed is a feedback because the Cp data is not constant. It depends on both the tip-speed ratio λ and the blade pitch angle β. After calculating λ the model uses the calculated λ and β as the input to the Cp look up table. This gives the current power coefficient of the turbine. This Cp value represents how efficiently the turbine extracts power from the wind under the present operating condition[7].

The main aim of the block is to estimate the wind speed. For the mathematical model the power equation is rearranged to obtain an equation for the wind speed. Referring to equ.3.3, the the rearranged equation for the wind speed estimation is stated as:

$$v = \sqrt[3]{\frac{2P_{\mathrm{m}}}{\rho A C_p}} \tag{3.7}$$

Note that this block contains a feedback loop because the estimated wind speed is used to calculate the tip-speed ratio λ, and λ is then used to determine the power coefficient C_p, which is again used to update the estimated wind speed. Therefore, the wind estimation block works as an iterative estimation structure in Simulink. In the feedback loop a Simulink block initial condition is used to avoid dividing with zero.

3.1.3.2 Model Block 2 – Power Estimation

The power estimation block is placed after the wind estimation block and uses the estimated wind speed as its main input. The available power estimation is carried out in two steps, where the wind speed is first estimated and then this estimated wind speed is used to calculate the available wind power. The estimated wind speed is used instead of the directly measured wind speed because it gives a better representation of the wind speed experienced by the turbine, since a wind-speed sensor can react more strongly to fast wind variations than the complete turbine system [7].

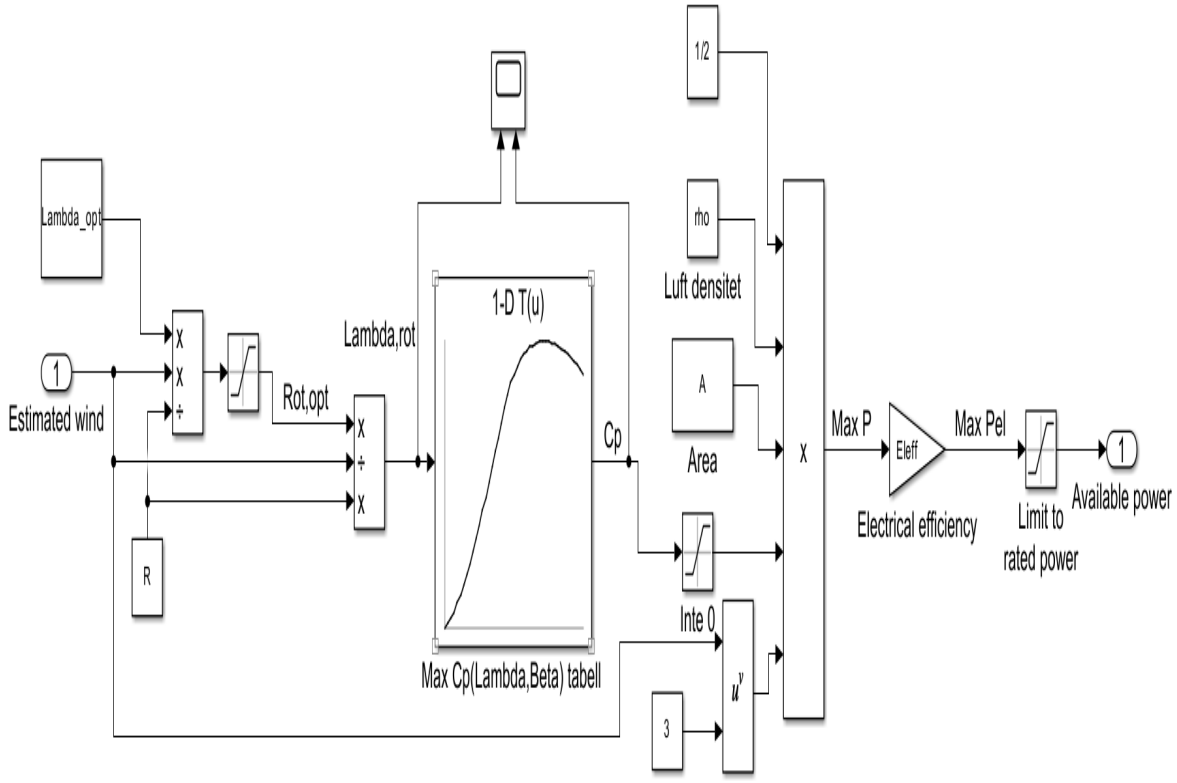


Figure 3.2: Power estimation block.

In this block, the optimum tip-speed ratio, λ_{opt}, is used to calculate the optimum rotor speed for the given wind speed. This is done to obtain the operating point where the turbine can extract the maximum possible power from the available wind [7]. The optimum rotor speed is calculated as:

$$\omega_{\text{opt}} = \frac{\lambda_{\text{opt}} v}{R} \tag{3.8}$$

where ω_{opt} is the optimum rotor speed, λ_{opt} is the optimum tip-speed ratio, v is the estimated wind speed, and R is the rotor radius. The calculated rotor speed is then limited so that it does not exceed the allowed rotational speed of the turbine. Based on this operating condition, the corresponding power coefficient, C_p, is obtained from the $C_p(\lambda, \beta)$ lookup table, since C_p depends on both the tip-speed ratio, λ, and the blade pitch angle, β[7].
The available mechanical power from the wind is then calculated using the wind power equation:

$$Pm = \frac{1}{2}\rho A C_p v^3 \tag{3.9}$$

where ρ is the air density, A is the rotor swept area, C_p is the power coefficient, and v is the estimated wind speed. Finally, the calculated mechanical power is converted into available electrical power by multiplying it with the electrical efficiency. The output is then limited to the rated turbine power so that the estimated available power does not exceed the turbine capacity[7].

3.1.3.3 Wind Turbine and Control System Implementation

The wind turbine and control system part includes DC-generator, NREL regulator, wind-spill controller, and power step control(PDF). The purpose of this block is to simulate and estimate the available wind power and the control system for the wind turbine. The available power represents the estimated maximum power that can generated from the available wind. In our model, we use this signal as the input reference for the wind spill block

The spill wind block reduces the turbine power output by producing MinPit and which is the minimum allowed blade pitch angle, and Spill factor from the spill wind block which help wind turbine to reduce power production and mainataining a desirable turbine speed[7].

The NREL regulator block which produces the generator ref torque and blade angle position based on turbine speed, current blade angle, Min Pit, and spill factor. The NREL block divide the operation of wind turbine into 3 different regions in region 1 which is the initial state or region where the wind energy is mainly used to accelerate the rotor. In region 2 the controller keep the turbine close to optimum tip-speed ratio, the torque reference helps maintain optimal aerodynamic efficiency. In region 3 to maintain the rotor speed near the rated condition the blade pitch angle is controlled to limit the produced power[7].

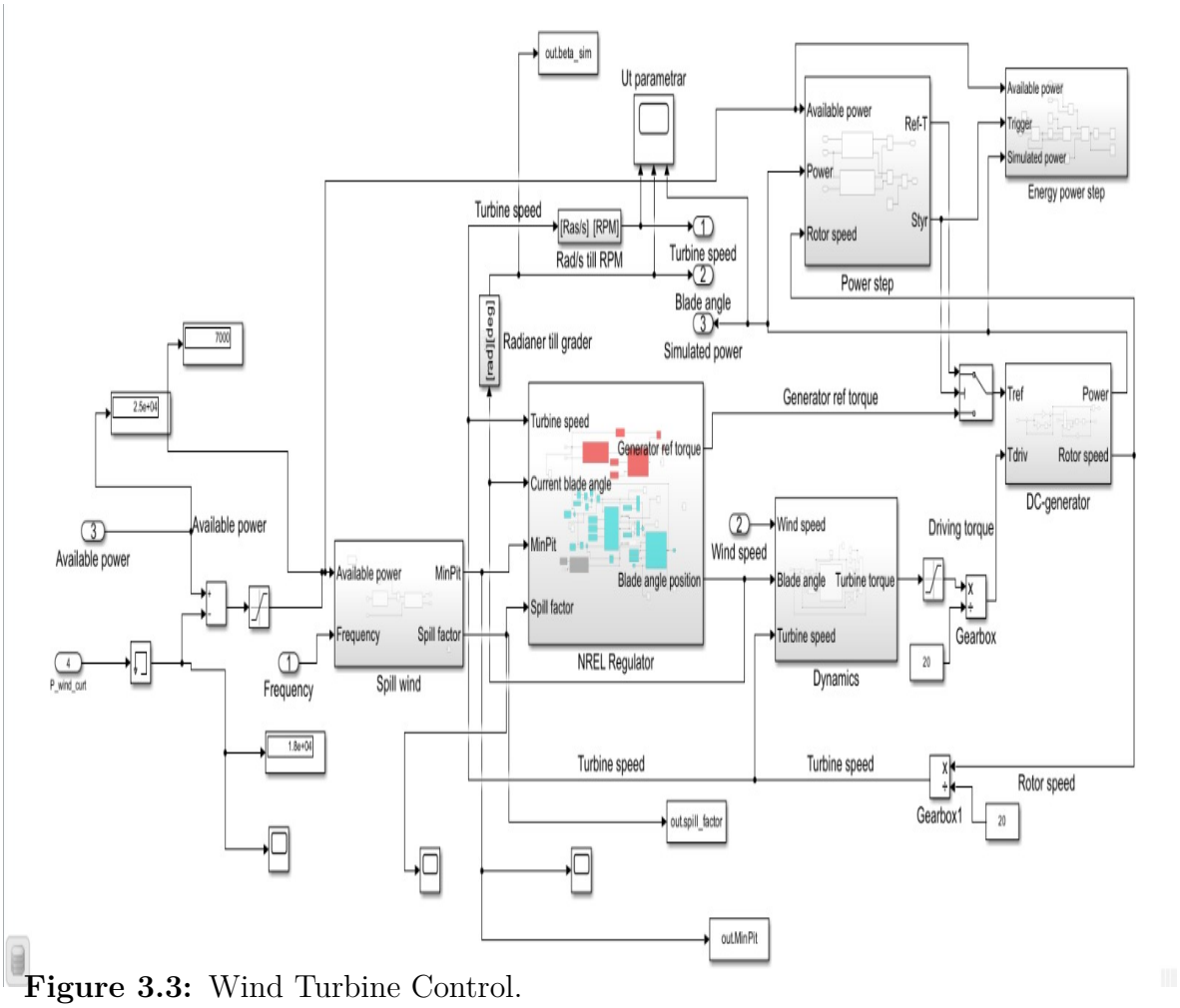


Figure 3.3: Wind Turbine Control.

The dynamics block comes next, which represent the aerodynamic part of the wind turbine for the calculation of the turbine driving torque from the input signal like wind speed, blade angle, and turbine speed, This block uses $C_p(\lambda, \beta)$ to calculate mechanical power from the wind then calculate the torque[7].
The generator block represents the generator dynamics and produces the simulated power and rotor speed from the input signals like generator reference torque from the controller and driving torque from the turbine(PDF). To create synthetic inertia or fast frequency response our model have a power step block basically a alternative torque for temporary power[7].

3.2 PV Model Development and Implementation

After going through different literature sources and studying different PV modelling approaches, a custom solar PV model was developed for this thesis. At the beginning, the available Simscape PV model was considered and tested. However, during the simulation work, it did not behave in the expected way for the islanded operation case. Also, using the built-in model added more complexity than what was actually required for this thesis. Because of this, a simplified but more realistic PV model was developed manually in Simulink using the single-diode equivalent circuit of a solar cell.

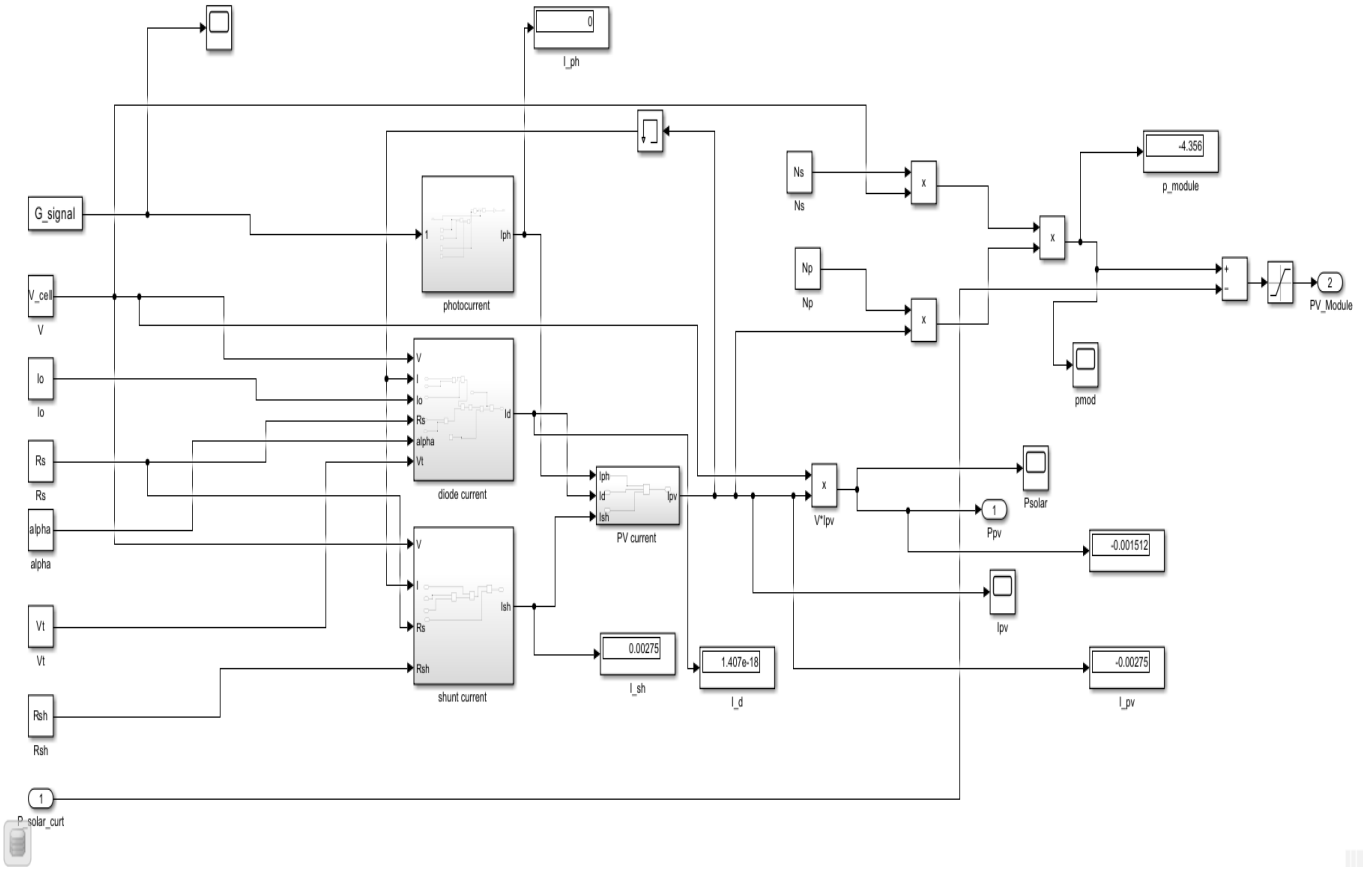


Figure 3.4: PV model implementation in Matlab.

The main reason for keeping the solar model simple is connected to the scope of this thesis. The main focus of the thesis is not detailed PV converter control, MPPT operation, or switching-level modelling. The main objective is to study the power balance in an islanded system and to develop an energy management strategy between the wind turbine, solar PV, battery, and load. Therefore, the PV model only needs to provide a reasonable solar power contribution that can be used by the power balance controller. For this reason, MPPT logic, DC-DC converter control, and detailed inverter control were not included in the model. Instead, the PV system was represented in a way that captures the effect of irradiance on solar power generation without making the overall system unnecessarily complex.
The PV model was built using the single-diode equivalent circuit because it gives a good balance between physical meaning and modelling simplicity. In this approach, the output current of the PV cell is obtained by considering the light-generated current and subtracting the internal loss currents. The basic equation used in the Simulink model is

$$I_{pv} = I_{ph} - I_d - I_{sh} \tag{3.10}$$

where I_{ph} is the photocurrent generated by solar irradiance, I_d is the diode current, and I_{sh} is the shunt current. Equation(3.10) was chosen because it clearly represents the current balance inside a PV cell. The current produced by sunlight is not fully

available at the output, because part of it is lost through the diode branch and the shunt branch. Therefore, this equation was suitable for representing the PV cell in a simple and logical way.
The photocurrent part of the model represents the current generated due to solar irradiance. In the simulation, the irradiance input is given as G, and the photocurrent is calculated as

$$I_{ph} = (I_{sc} + K_{sc}(T - T_{ref}))\,\frac{G}{1000} \tag{3.11}$$

where I_{sc} is the short-circuit current, K_{sc} is the temperature coefficient of the short-circuit current, T is the operating temperature, and T_{ref} is the reference temperature. Equation(3.11) was used because irradiance is the main factor that changes the solar power output. The temperature term is also included, but its effect is smaller compared to irradiance. In this thesis model, this part is important because the PV power should change according to the available solar irradiance and then contribute to the overall energy balance of the islanded system.
The diode current was implemented using the exponential diode equation,

$$I_d = I_o\left(e^{\frac{V+I_{pv}R_s}{\alpha V_t}} - 1\right) \tag{3.12}$$

where I_o is the diode saturation current, V is the PV cell voltage, R_s is the series resistance, α is the diode ideality factor, and V_t is the thermal voltage. Equation(3.12) part of the model represents the nonlinear behaviour of the solar cell. The diode equation is important because a PV cell does not behave as a simple linear current source. Its current and voltage relationship is nonlinear, and this behaviour is mainly represented by the diode branch. Since I_{pv} appears inside this equation, the model requires a feedback path in Simulink. To avoid direct algebraic-loop issues during simulation, a Memory block was added in the feedback path.
The shunt current was calculated using

$$I_{sh} = \frac{V + I_{pv}R_s}{R_{sh}} \tag{3.13}$$

where R_{sh} is the shunt resistance. This term represents the leakage current inside the PV cell. In a practical solar cell, not all generated current reaches the output terminals, because a small part of the current can flow through internal leakage paths. The shunt branch was therefore included to make the model more realistic than a simple irradiance-to-power block.
After calculating I_{ph}, I_d, and I_{sh}, the output current I_{pv} was obtained using the current balance equation. The cell-level power was then calculated as

$$P_{pv} = V \times I_{pv} \tag{3.14}$$

The model was first developed at the cell level, because this made the equation implementation clearer and easier to understand. After that, scaling was added to represent the required PV module or array size. The number of series-connected cells is represented by N_s, and the number of parallel strings is represented by N_p. Therefore, the final scaled solar power was calculated as

$$P_{\text{module}} = (N_s V)(N_p I_{pv}) \tag{3.15}$$

This scaling method Equation.(3.15) made it possible to use the same cell-level model for different PV power ratings by changing N_s and N_p. For example, the model can be scaled to represent a higher solar power level required for the islanded system. This is useful for the thesis because the power balance controller only needs the solar power contribution from the PV system, rather than detailed MPPT or converter-level behaviour.

Overall, the developed PV model provides a simple but realistic solar power input for the islanded operation study. The model includes the main physical effects of a PV cell, such as irradiance-dependent photocurrent, diode behaviour, and shunt leakage. At the same time, it avoids unnecessary control complexity. This makes the model suitable for the main aim of the thesis, which is to analyse energy management and power balancing between the wind turbine, solar PV, battery, and load during islanded operation.

3.3 Battery Energy Storage System Model

The battery system in the Simulink model is implemented as a simplified power-based energy storage model. The input to this block is the battery power reference, $P_{\text{bat,ref}}$, which represents the required charging or discharging power from the energy management system. Before the reference is applied to the battery model, it is passed through a battery power limit block. This limiter is used to keep the battery power within the allowed operating range and to avoid unrealistic charging or discharging values in the simulation.

After limiting the reference power, the battery current is calculated using the battery voltage. The relation used in the block can be written as

$$I_{\text{bat}} = \frac{P_{\text{bat}}}{V_{\text{bat}}} \tag{3.16}$$

where I_{bat} is the battery current, P_{bat} is the limited battery power, and V_{bat} is the battery voltage. In the model, the sign convention is handled using gain blocks, so that the direction of the battery current and energy flow follows the charging and discharging logic of the system.

The state of charge is obtained by integrating the battery current with respect to time. This represents the change in battery charge during operation.

A gain block is used to convert the integrated current into the SOC value, and a saturation block is then applied to keep the SOC within its physical limits. This is necessary because the SOC of a battery cannot exceed the maximum value or fall below the minimum allowed value.

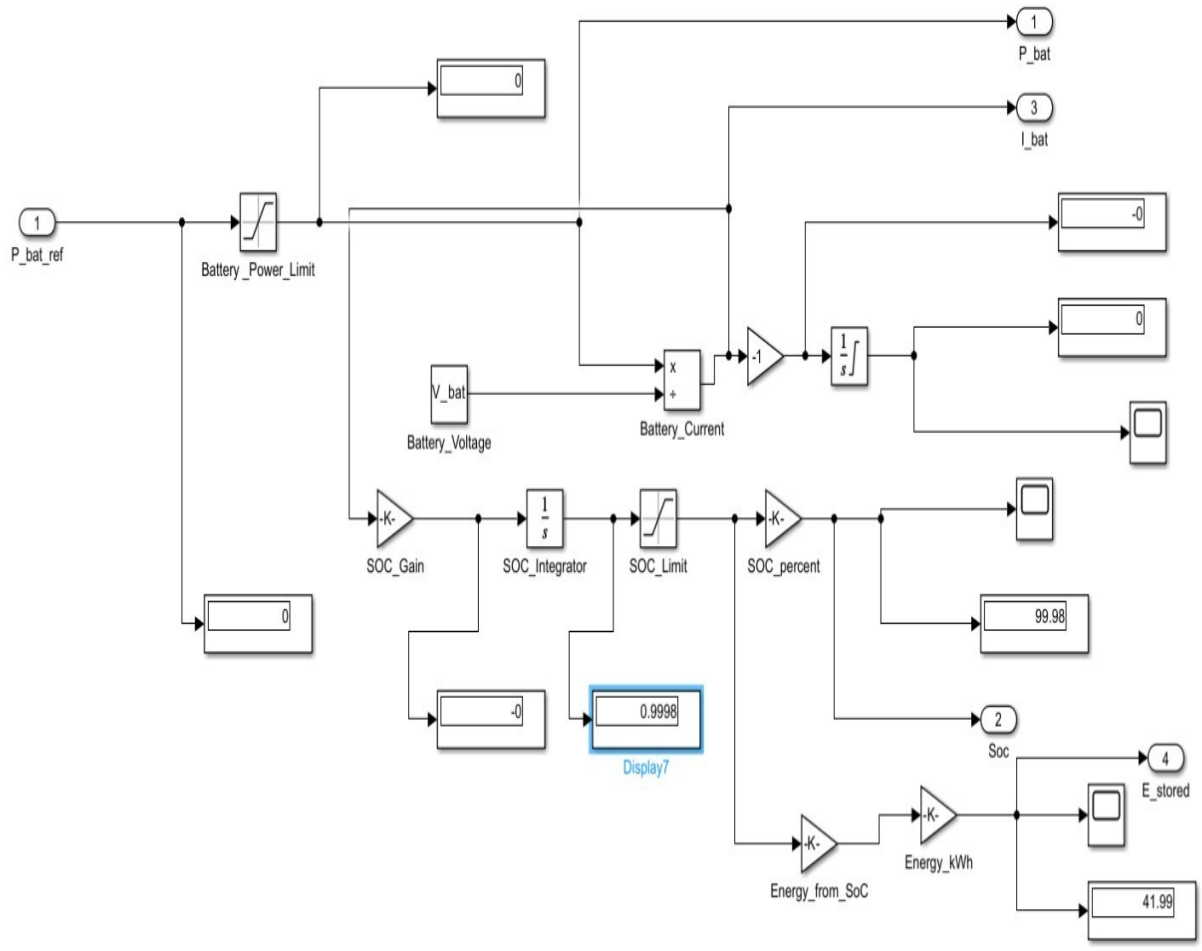


Figure 3.5: Battery energy storage system model.

The SOC is also converted into percentage form using the SOC percent gain block. This makes it easier to observe the battery condition during the simulation. In addition, the block calculates the stored energy of the battery from the SOC value. The stored energy output, E_{stored}, gives an indication of how much energy is available in the battery at each time step.

The outputs of this battery subsystem are the battery power P_{bat}, battery current I_{bat}, state of charge SOC, and stored energy E_{stored}. These outputs are useful for checking whether the battery is charging or discharging correctly and whether the battery has enough stored energy to support the islanded power balance. Since the main aim of the model is to study power balancing in an islanded wind–PV–battery system, this simplified battery model is suitable because it focuses on the power, current, SOC, and stored-energy behaviour rather than detailed electrochemical battery dynamics.

3.4 Energy Management System for Wind–PV–Battery Power Balance

The Energy Management System (EMS) was developed as the supervisory control layer of the islanded wind–PV–battery system, where its main function is to coordinate the renewable generation, battery operation, and load demand [23],[26].
In a hybrid renewable microgrid, an EMS is required because wind power, solar power, and load demand vary with time, which continuously creates a mismatch between generation and consumption. [25, 26]
Energy storage is normally included in renewable microgrids because the battery can absorb surplus power during high renewable generation and supply power during renewable power shortage [26],[27].
The EMS therefore acts as the decision-making part of the system by checking the available renewable power, the load demand, and the battery state of charge before selecting the required battery operating mode [23][24].
In the implemented Simulink model, the total renewable power is calculated from the wind turbine power and the photovoltaic power as shown in Equation(3.17) [27],[23].

$$P_{ren} = P_{wind} + P_{PV} \tag{3.17}$$

The power mismatch is then calculated by comparing the load demand with the available renewable power as shown in Equation(3.18) [26],[27].

$$P_{bat,ref} = P_{load} - P_{ren} \tag{3.18}$$

The general active power balance of the islanded system can be expressed as shown in Equation(3.19) [27],[28].

$$P_{wind} + P_{PV} + P_{bat} = P_{load} \tag{3.19}$$

In this equation, the battery power becomes positive during discharge and negative during charge depending on the sign convention used in the simulation model [27],[28].
When $P_{bat,ref} > 0$, the renewable generation is lower than the load demand, and the EMS commands the battery to discharge in order to supply the missing power[23],[27].
When $P_{bat,ref} < 0$, the renewable generation is higher than the load demand, and the EMS commands the battery to charge using the surplus renewable power[23],[27].
When $P_{bat,ref} = 0$, the renewable generation is approximately equal to the load demand, and the battery remains nearly idle because no balancing power is required[26],[27].
The battery operation is limited by the state of charge constraints in order to avoid overcharging and deep discharging[24],[27].
In this study, the minimum and maximum SOC limits are selected as 10% and 90%, respectively, so the EMS blocks further discharge at the lower SOC limit and blocks further charge at the upper SOC limit [24].
The SOC constraint used in the EMS can be written as shown in Equation 3.20[24],[27].

$$SOC_{min} \leq SOC \leq SOC_{max} \tag{3.20}$$

The charging and discharging powers are also limited by the maximum battery power rating so that the EMS does not request unrealistic battery power during large renewable or load variations [27],[28].

The battery power constraint can be expressed as shown in Equation 3.21[28].

$$-P_{ch,max} \leq P_{bat,ref} \leq P_{dis,max} \tag{3.21}$$

During surplus operation, the EMS first checks whether the battery SOC is below the maximum limit before allowing the battery to charge [23],[27].

If the battery reaches the maximum SOC limit while renewable generation is still higher than the load demand, the battery cannot absorb more energy and the remaining excess power must be reduced through renewable power limitation or curtailment[23],[27].

During deficit operation, the EMS first checks whether the battery SOC is above the minimum limit before allowing the battery to discharge. [24],[27]

If the battery reaches the minimum SOC limit while renewable generation is still lower than the load demand, the EMS prevents further battery discharge to protect the battery from deep discharge [27],[24].

In a practical islanded system, this condition would require load reduction, another backup source, or additional power support because the available renewable power and usable battery power are not enough to supply the full load[23],[24].

The EMS logic used in this thesis is therefore a rule-based power balancing method rather than an optimization-based energy management method[25],[26].

This approach is suitable for the present Simulink study because the main aim is to analyse the power balance between wind generation, PV generation, battery response, and load demand in islanded operation[26],[27].

Rule-based EMS methods are useful for this type of study because the operating decisions are clear, easy to implement, and directly related to the measured power mismatch and SOC limits[25],[26].

More advanced EMS methods such as model predictive control, convex optimization, artificial intelligence, and multi-agent control are also used in the literature for cost optimization, forecasting, market participation, and complex scheduling[28],[25],[26].

However, the EMS in this thesis is mainly focused on direct active power balancing and SOC-based battery operation, which makes the control structure simpler and more suitable for the islanded system analysis[23],[27].

Overall, the implemented EMS continuously compares renewable generation with load demand and decides whether the battery should charge, discharge, or remain idle[26],[27].

By using this logic, the battery stores surplus wind and PV power during high renewable generation and supports the load during low renewable generation[23],[27].

Therefore, the developed EMS provides a logical control structure for maintaining active power balance in the islanded wind–PV–battery system while keeping the battery operation within safe SOC and power limits. [24, 27, 28]

3.5 Grid-Forming Converter Control Implementation

In the islanded wind–solar–battery system considered in this work, the battery converter is required to establish and maintain the AC bus voltage independently, since no external grid is available to define system frequency and voltage. To this end, a simplified grid-forming control strategy was developed for the battery converter. The approach is based on the grid-forming principles described by Narula [16], in which a grid-forming converter is treated as a controllable voltage source that establishes its own voltage magnitude, frequency, and phase angle, rather than synchronizing to an external voltage through a phase-locked loop.
This distinction is central to the control design. A grid-following converter injects a commanded current into a voltage that has already been established elsewhere in the network. A grid-forming converter, by contrast, must generate that voltage itself; consequently, the stability of the entire islanded system depends on the converter performing this function correctly. Without a unit capable of forming the bus voltage, no stable frequency or voltage reference would exist for the remaining generation units to synchronize to.
The control structure was implemented in EMTPWorks using two coordinated control loops: an active-power control loop and a voltage-reference control loop. The active-power loop generates the converter phase angle directly from the active-power balance, which corresponds to the mechanism used by grid-forming converters to achieve synchronization without a phase-locked loop[29, 34].

3.5.1 Active-Power Loop

The active-power reference P_g^* and the measured converter active power P_g are first converted to per-unit values using the converter's rated apparent power S_N. The active-power error is then obtained as Equation(3.22)

$$e_p = \frac{P_g^*}{S_N} - \frac{P_g}{S_N} \tag{3.22}$$

This error is processed by a PI controller to generate a frequency-correction term. An active-damping term, proportional to the measured active power, is additionally incorporated to improve the dynamic response of the converter which can be seen in Equation(3.23), consistent with the damping mechanism employed in the reference grid-forming controller.
The resulting converter angular frequency is given by Equation(3.23)

$$\omega_c = \omega_N + \left(K_{p,pc} + \frac{K_{i,pc}}{s}\right) e_p - R_a \frac{P_g}{S_N} \tag{3.23}$$

where ω_N denotes the nominal angular frequency, $K_{p,pc}$ and $K_{i,pc}$ are the proportional and integral gains of the active-power controller, and R_a is the active-damping gain. Integration of ω_c yields the converter phase angle Equation(3.23):

$$\theta_c = \int \omega_c \, dt \tag{3.24}$$

The angle θ_c constitutes the principal output of the active-power controller, as it determines the phase position of the converter voltage reference. In the EMTPWorks implementation, this angle is used to generate three balanced sinusoidal voltage references for the three-level voltage-source converter (VSC), which are shown in Equations(3.25),(3.26),(3.27)

$$v_a^* = E_{ref}\cos(\theta_c) \tag{3.25}$$

$$v_b^* = E_{ref}\cos\left(\theta_c - \frac{2\pi}{3}\right) \tag{3.26}$$

$$v_c^* = E_{ref}\cos\left(\theta_c + \frac{2\pi}{3}\right) \tag{3.27}$$

Here, E_{ref} denotes the voltage reference magnitude. These reference signals are supplied to the Vref input of the three-level converter block in EMTPWorks. As the converter model operates on a per-unit basis, the generated voltage references are likewise expressed in per-unit form.

3.5.2 Voltage-Reference Loop

A voltage-control loop was implemented to regulate the magnitude of the converter voltage. The measured three-phase voltage v_a, v_b, v_c is transformed into a rotating $dq0$ reference frame as Equation(3.28), synchronized to the converter angle θ_c obtained from the active-power loop:

$$\begin{bmatrix} v_d \\ v_q \\ v_0 \end{bmatrix} = \frac{2}{3}\begin{bmatrix} \cos(\theta_c) & \cos\left(\theta_c - \frac{2\pi}{3}\right) & \cos\left(\theta_c + \frac{2\pi}{3}\right) \\ -\sin(\theta_c) & -\sin\left(\theta_c - \frac{2\pi}{3}\right) & -\sin\left(\theta_c + \frac{2\pi}{3}\right) \\ \frac{1}{2} & \frac{1}{2} & \frac{1}{2} \end{bmatrix}\begin{bmatrix} v_a \\ v_b \\ v_c \end{bmatrix} \tag{3.28}$$

where the 2/3 scaling factor corresponds to the amplitude-invariant Park transformation. The magnitude of the measured converter voltage is then obtained from the d- and q-axis components as Equation(3.29),

$$E_{meas} = \sqrt{v_d^2 + v_q^2} \tag{3.29}$$

The voltage magnitude error is calculated with respect to a per-unit voltage set-point E^* (nominal value of unity in per-unit) as

$$e_v = E^* - E_{meas} \tag{3.30}$$

This error is processed through a PI controller to generate the voltage reference magnitude Equation(3.31):

$$E'_{ref} = \left(K_{p,vc} + \frac{K_{i,vc}}{s}\right)e_v \tag{3.31}$$

where $K_{p,vc}$ and $K_{i,vc}$ are the proportional and integral gains of the voltage controller. The controller output is then bounded by a saturation block to obtain the final voltage reference magnitude Equation(3.32):

$$E_{ref} = \begin{cases} E_{ref,max}, & E'_{ref} > E_{ref,max} \\ E'_{ref}, & E_{ref,min} \leq E'_{ref} \leq E_{ref,max} \\ E_{ref,min}, & E'_{ref} < E_{ref,min} \end{cases} \tag{3.32}$$

This limitation, expressed in Equation (3.32), ensures that the reference magnitude E_{ref} does not exceed the safe modulation range of the converter before being multiplied by the three-phase cosine terms defined in Equations (3.25)–(3.27).

3.5.3 Overall Control Structure

Figure 3.6 presents the complete control structure as implemented in EMTPWorks. The upper portion of the diagram corresponds to the active-power loop, in which P_g^* and P_g are converted to per-unit values, compared, processed through the PI controller, and combined with the nominal angular frequency and the damping term to generate ω_c; this quantity is subsequently integrated to obtain the converter angle θ_c. The lower portion of the diagram corresponds to the voltage-reference loop, in which the voltage magnitude is regulated and used to scale the generated three-phase voltage references.

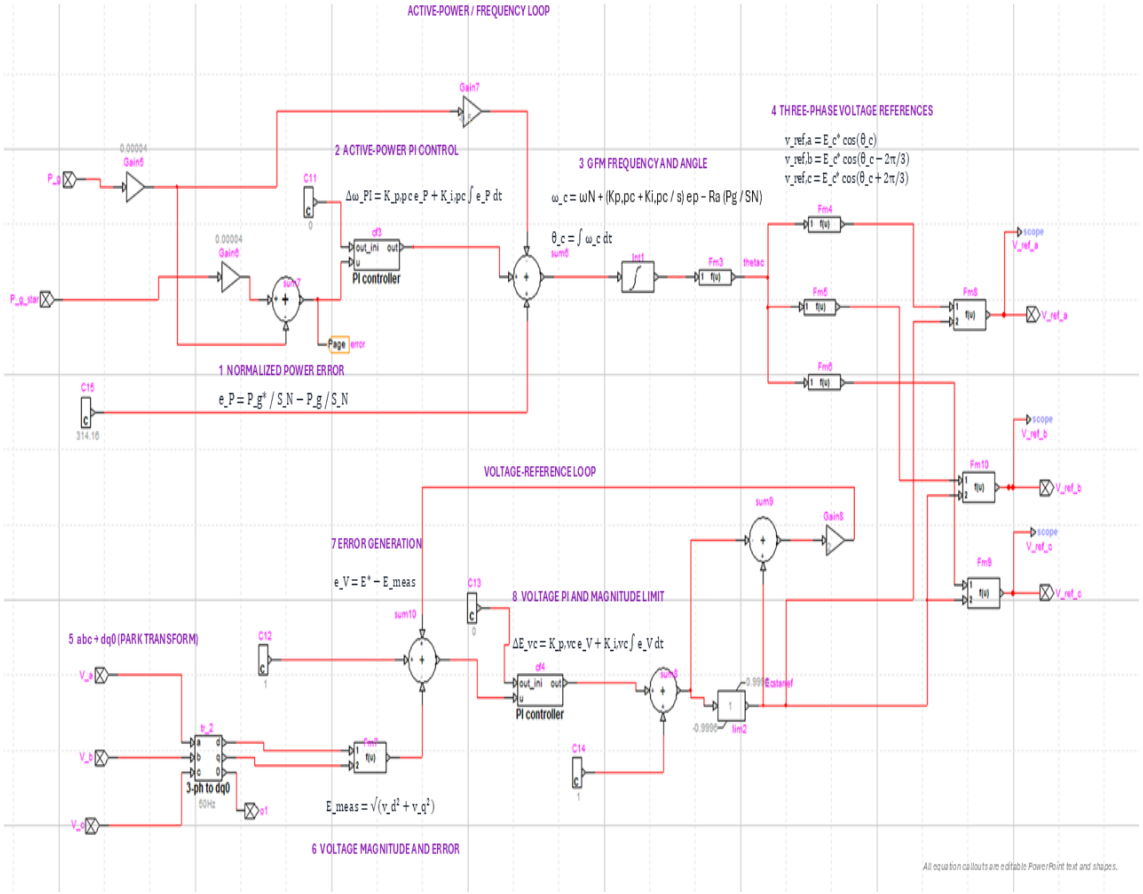


Figure 3.6: EMTP implementation of the grid-forming converter control structure.

It should be emphasized that the controller presented here constitutes a simplified

representation of the grid-forming structure described in the reference thesis. The complete controller in the reference work additionally incorporates virtual admittance, detailed current-limiting mechanisms, inertia-emulation loops, and a dedicated tuning procedure intended for grid-connected converter systems. These elements were not required for the present study, as its objective differed from that of the reference work.
Accordingly, the developed model retains only the essential grid-forming functionality required for the system under study: generation of an internal frequency, integration of this frequency into a converter phase angle, and use of this angle to construct the three-phase voltage reference for the battery converter. This structure enables the battery converter to support the islanded AC bus while the wind and solar generation units supply variable active power to the system

3.5.4 Overall Test Setup for GFM-Based Islanded Operation

The complete EMTPWorks model used to evaluate the grid-forming converter is presented in Figure 3.7. The main purpose of this test arrangement was to investigate whether the battery-supported converter could maintain the local AC system after disconnection from a stiff external grid. During the initial stage of the simulation, the external AC source establishes the voltage and frequency at the point of common coupling (PCC). Once the system reaches its initial operating condition, the source is disconnected and the battery converter is required to take over the voltage- and frequency-forming role.
EMTPWorks was used as the graphical environment for assembling the network components, converter models, control blocks, measurements, and switching logic required for the simulation [29]. The overall model consists of a battery energy storage system, a DC–DC boost converter, a DC-link capacitor, an average-value voltage-source converter (VSC), an RL filter, a three-phase load, measurement blocks, switching elements, and the developed grid-forming controller.
The battery and DC–DC converter were included mainly to provide the required DC-side supply for the VSC. Their detailed internal design was not part of the main scope of this study. Instead, generic EMTPWorks blocks were used so that a suitable and sufficiently regulated DC-link voltage could be provided to the AC-side converter. The DC-link capacitor acts as an intermediate energy-storage element between the battery-side converter and the VSC, helping to decouple the two converter stages during dynamic operation.
The DC–DC boost converter was therefore used primarily to maintain the DC-link voltage at the level required by the VSC. Since the objective of the study was focused on the grid-forming behaviour on the AC side, a detailed analysis or tuning of the boost-converter control was not carried out. Its role was limited to supporting the converter during the GFM validation tests [30].
On the AC side, the converter was represented using an average-value VSC model. This type of model describes the averaged electrical behaviour of the converter without explicitly simulating the individual semiconductor switching events. Such a representation reduces the computational complexity of the simulation and is

suitable when the main interest is in the control dynamics, power exchange, PCC-voltage behaviour, and the transition between grid-connected and islanded operation rather than in switching harmonics or device-level transients [30, 31].
A three-phase PQ load was connected to the 400 V line-to-line RMS AC bus. For the presented validation case, the active-power demand was set to

$$P_{\text{load}} = 20 \text{ kW}, \tag{3.33}$$

while the reactive-power demand was selected as

$$Q_{\text{load}} = 0 \text{ kVAr}. \tag{3.34}$$

This corresponds to an approximately unity-power-factor load. The choice of $Q_{\text{load}} = 0$ was intentional because the power-management strategy investigated in this work is based mainly on the active-power balance between the load, renewable generation, and battery converter.
The active-power reference supplied to the GFM converter is calculated by the power-balance controller as

$$P_g^* = P_{\text{load}} - P_{\text{Stiff}} \tag{3.35}$$

where P_g^* is the active-power reference of the battery converter, P_{load} is the local load demand, P_{Stiff} is the available power from the stiff AC source.
According to Equation (3.35), the battery converter supplies the power deficit whenever the total renewable generation is lower than the load demand. If the renewable generation exceeds the demand, the sign of the calculated reference changes and the battery can absorb the excess power, depending on the sign convention implemented in the simulation model. Here for testing we have considered one condition which is similar to the deficit condition.
Reactive power was not included in the power-balance equation because the developed energy-management logic was intended to determine the real-power exchange required from the battery. The validation case was therefore simplified by setting the reactive load demand to zero. This makes it easier to evaluate the response of the active-power controller and the frequency-forming behaviour without introducing an additional reactive-power disturbance.
This assumption should not be interpreted as implying that reactive-power control is unnecessary in a practical grid-forming converter. In a complete GFM system, reactive-power demand and voltage–reactive-power characteristics can influence voltage regulation and power sharing. However, detailed reactive-power control was outside the scope of the present test, which was primarily intended to assess the active-power balance, voltage establishment, frequency formation, and islanding response of the battery converter.
At the beginning of the simulation, the PCC remains connected to a stiff three-phase AC source. During this period, the external source fixes the voltage and frequency of the AC network and provides a stable initial operating point. After the selected switching instant, the connection between the stiff source and the PCC is opened. The local network then becomes electrically islanded, and the battery converter is required to maintain the AC bus without support from the external grid.

This switching sequence provides a direct way of demonstrating the transition from grid-supported operation to converter-formed operation. Before islanding, the PCC voltage angle and frequency are imposed by the external source. After disconnection, the converter can no longer rely on the stiff grid and must generate the electrical quantities required to support the local network.
The active-power reference calculated by the power-balance controller is supplied to the GFM active-power control loop. The measured converter active power is compared with the reference, and the resulting power error is used by the developed controller to determine the converter angular-frequency behaviour. The angular frequency is then integrated to obtain the converter phase angle Equation(3.36),

$$\theta(t) = \int \omega(t)\, dt. \tag{3.36}$$

In parallel with the active-power loop, the voltage-reference loop regulates the magnitude of the converter output voltage. The voltage-magnitude reference and the internally generated phase angle are then combined to produce the three-phase converter voltage references,

$$v_{\mathrm{ref},a}, \qquad v_{\mathrm{ref},b}, \qquad v_{\mathrm{ref},c}. \tag{3.37}$$

These signals are applied to the voltage-reference input of the average-value VSC.
The main difference from a grid-following converter is that the converter does not depend on a phase-locked loop to continuously track an externally imposed grid angle during islanded operation. Instead, the GFM controller develops its own voltage magnitude, phase angle, and frequency reference. In this way, the converter operates as a controllable AC voltage source and is capable of establishing the electrical reference for the local islanded system [16].
The overall active-power control structure can therefore be summarised as

$$P_{\mathrm{load}} - P_{\mathrm{stiff}} \rightarrow P_g^* \rightarrow \text{GFM active-power controller} \rightarrow \omega \rightarrow \theta. \tag{3.38}$$

The voltage-regulation path can similarly be represented as

$$V^* - V_{\mathrm{PCC}} \rightarrow \text{Voltage-reference controller} \rightarrow V_{\mathrm{ref}}. \tag{3.39}$$

The internally generated voltage magnitude and phase angle are then used to form the three-phase voltage references applied to the VSC.
The purpose of this overall test arrangement is to verify that the developed GFM controller can continue supporting the local network after the stiff AC source is removed. Particular attention is given to whether the converter can restore and maintain the PCC voltage, establish a stable operating frequency, and supply the active-power deficit determined by the power-balance controller. The main quantities monitored during the simulation include the PCC voltage, converter current, active power, system frequency, DC-link voltage, and battery response. These variables are subsequently used to assess the performance of the converter during the transition to islanded operation.

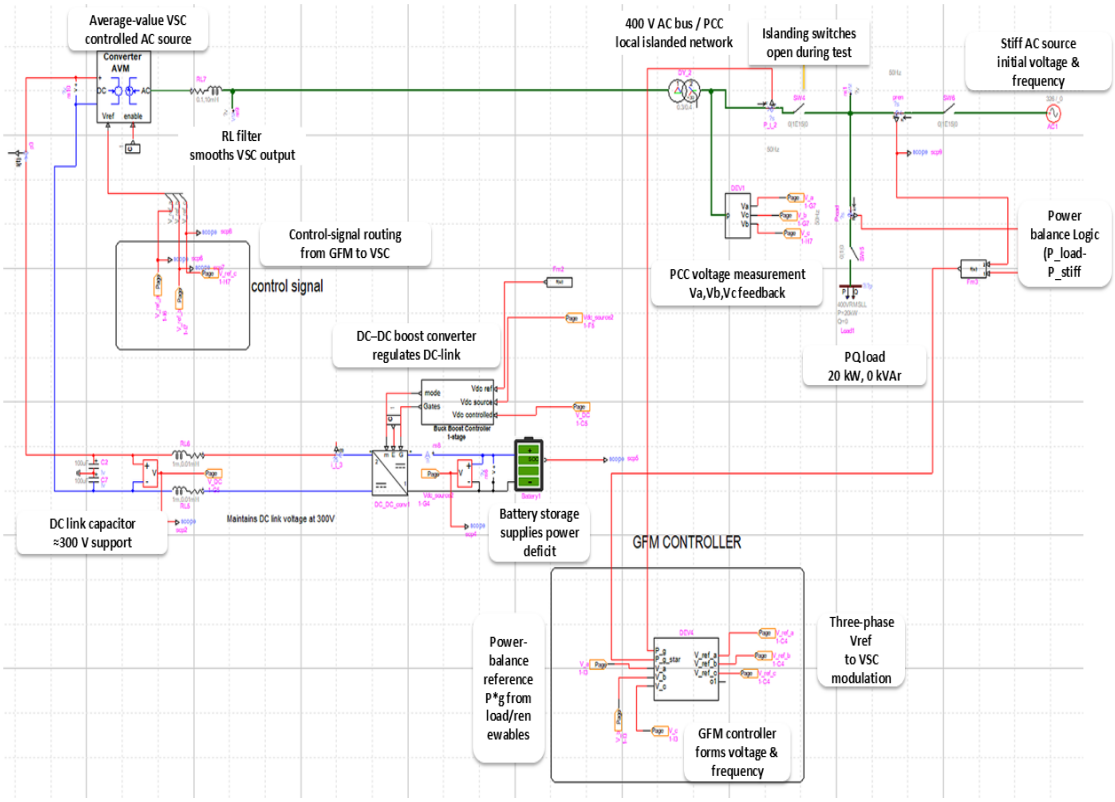


Figure 3.7: Overall EMTPWorks test setup used to validate GFM-based islanded operation.

3.6 PLL Controller Implementation for the Grid-Following Converter

The grid-following (GFL) converter requires information about the electrical angle and frequency of the AC system in order to remain synchronized with the voltage at the point of common coupling (PCC). In this study, this synchronization is achieved using a phase-locked loop (PLL). PLL-based synchronization is widely used in three-phase converter systems because it allows the controller to estimate the phase angle and frequency directly from the measured AC voltage [32, 33].

An important distinction should be made between the roles of the grid-forming and grid-following converters in the islanded system considered in this work. After islanding, the PCC voltage and frequency are established by the grid-forming (GFM) converter. The PLL of the grid-following converter therefore does not regulate the PCC voltage or determine the system frequency. Its purpose is to observe the voltage already established at the PCC and determine its instantaneous phase angle and frequency. The estimated angle is then used by the GFL converter to keep its internal reference frame and converter reference signals synchronized with the islanded AC bus.

The PLL implemented in EMTP uses the measured three-phase PCC voltages v_a, v_b, and v_c as its input signals. These voltages can be written in vector form as

$$\mathbf{v}_{abc,\mathrm{PCC}} = \begin{bmatrix} v_a \\ v_b \\ v_c \end{bmatrix}. \tag{3.40}$$

To obtain suitable signals for phase detection, the measured three-phase quantities are first converted into a stationary two-axis reference frame. Using the Clarke transformation, the α- and β-axis voltage components are calculated as shown in Equations (3.41) and (3.42).

$$v_\alpha = \frac{2}{3}\left(v_a - \frac{1}{2}v_b - \frac{1}{2}v_c\right), \tag{3.41}$$

and

$$v_\beta = \frac{2}{3}\left(\frac{\sqrt{3}}{2}v_b - \frac{\sqrt{3}}{2}v_c\right). \tag{3.42}$$

The stationary $\alpha\beta$ quantities are subsequently transformed into a rotating dq reference frame. The transformation is performed using the estimated PLL angle, θ_{PLL}, which is continuously updated by the PLL feedback loop. The resulting components are given in Equations (3.43) and (3.44).

$$v_d = v_\alpha \cos(\theta_{\mathrm{PLL}}) + v_\beta \sin(\theta_{\mathrm{PLL}}), \tag{3.43}$$

$$v_q = -v_\alpha \sin(\theta_{\mathrm{PLL}}) + v_\beta \cos(\theta_{\mathrm{PLL}}). \tag{3.44}$$

This synchronous-reference-frame approach provides a convenient way of identifying the phase difference between the measured voltage vector and the reference frame used by the controller [32, 33]. When the estimated reference frame becomes aligned with the PCC voltage vector, the voltage appears mainly on the d-axis, while the quadrature component approaches zero. Therefore, the PLL attempts to satisfy the condition expressed in Equation (3.45).

$$v_q \approx 0. \tag{3.45}$$

3.6.1 Generation of the d-axis Current Reference

In the grid-following converter control, the active power reference is converted into a d-axis current reference. The function implemented in EMTP is written as:

$$i_d^* = \frac{2u[1]}{3\left(|u[2]| + 1\right)} \tag{3.46}$$

where the EMTP function block expression is:

```
2*u[1]/(3*(ABS(u[2])+1))
```
(3.47)

Here, the input variables are defined as:

$$u[1] = P^* \tag{3.48}$$

$$u[2] = v_d \tag{3.49}$$

Therefore, the implemented equation can be written as Equation(3.50):

$$i_d^* = \frac{2P^*}{3\left(|v_d| + 1\right)} \tag{3.50}$$

In Equation(3.50) i_d^* is the d-axis current reference, P^* is the active power reference, and v_d is the d-axis component of the PCC voltage obtained from the abc-to-dq transformation using the PLL angle.
The active power in the dq reference frame is given by Equation(3.51):

$$P = \frac{3}{2}\left(v_d i_d + v_q i_q\right) \tag{3.51}$$

In a PLL-synchronized grid-following converter, the d-axis is aligned with the PCC voltage vector. Therefore, after synchronization, the q-axis voltage becomes approximately zero:

$$v_q \approx 0 \tag{3.52}$$

As a result, the active power equation can be simplified to:

$$P \approx \frac{3}{2} v_d i_d \tag{3.53}$$

Rearranging this Equation(3.53) gives the d-axis current reference required to inject the desired active power Equation(3.54):

$$i_d^* = \frac{2P^*}{3v_d} \tag{3.54}$$

In the implemented EMTP function, the absolute value of v_d is used:

$$|v_d| \tag{3.55}$$

This is included to avoid sign errors caused by the selected dq transformation convention. Depending on the phase sequence and angle reference, the calculated v_d may appear as a negative value even though the voltage magnitude is correct. Using $|v_d|$ ensures that the current reference is calculated based on the voltage magnitude. The additional value of +1 in the denominator is included for numerical protection:

$$|v_d| + 1 \tag{3.56}$$

This prevents division by zero or very small voltage values during the start-up period of the simulation, before the PLL has fully synchronized and before the PCC voltage has reached a stable value.
The error is supplied to a proportional-integral (PI) controller. The PI controller responds to any difference between the estimated reference-frame angle and the actual PCC voltage angle. Its output is interpreted as a correction to the nominal angular frequency and is denoted by

$$\Delta\omega. \tag{3.57}$$

A limiter is placed after the PI controller to prevent an unrealistically large frequency correction during transients or during the initial synchronization process. For the model developed in this study, the correction is restricted to the range specified in Equation (3.58).

$$-31.4 \leq \Delta\omega \leq +31.4 \quad \text{rad/s}. \tag{3.58}$$

The frequency deviation is calculated using Equation (3.59).

$$\Delta f = \frac{\Delta\omega}{2\pi}, \tag{3.59}$$

A limit of 31.4 rad/s corresponds to approximately 5 Hz. Therefore, the selected limiter allows a maximum PLL frequency correction of approximately ±5 Hz around the nominal operating frequency.
The nominal system frequency considered in the simulation is given in Equation (3.60).

$$f_0 = 50 \text{ Hz}. \tag{3.60}$$

The corresponding nominal angular frequency is therefore expressed in Equation (3.61).

$$\omega_0 = 2\pi f_0, \tag{3.61}$$

which gives the result shown in Equation (3.62)

$$\omega_0 = 2\pi(50) = 314.16 \text{ rad/s}. \tag{3.62}$$

The output of the PI controller does not directly represent the complete angular frequency of the PLL. Instead, it represents the deviation from the nominal value. The estimated PLL angular frequency is consequently calculated by adding the limited correction term to the nominal angular frequency, as shown in Equation (3.63)

$$\omega_{\text{PLL}} = \omega_0 + \Delta\omega. \tag{3.63}$$

The estimated electrical angle is then obtained by integrating the angular frequency, as shown in Equation (3.64)

$$\theta_{\text{PLL}} = \int \omega_{\text{PLL}}\, dt. \tag{3.64}$$

This angle is returned to the *dq*-transformation block and therefore closes the PLL feedback loop. If the estimated angle differs from the actual PCC voltage angle, a non-zero v_q component is produced. The PI controller then modifies $\Delta\omega$, which changes ω_{PLL} and consequently adjusts θ_{PLL}. As the estimated reference frame approaches the PCC voltage angle, the magnitude of v_q decreases. This feedback mechanism allows the PLL to continuously follow variations in the phase and frequency of the measured AC voltage, which is the fundamental operating principle of synchronous-reference-frame PLL synchronization [32, 33].

Once the PLL has reached a synchronized condition, the rotating reference frame is aligned with the PCC voltage vector. Under this condition,

$$v_q \approx 0, \tag{3.65}$$

while the d-axis component contains the main voltage component in the aligned reference frame.

In addition to providing the synchronization angle for the reference-frame transformation, θ_{PLL} is also used to generate the three-phase reference signals required by the two-level voltage-source converter (VSC). For the initial implementation used in this work, balanced sinusoidal reference signals are generated according to Equations(3.66),(3.67),(3.68):

$$v_{a,\mathrm{ref}} = 0.8 \sin(\theta_{\mathrm{PLL}}), \tag{3.66}$$

$$v_{b,\mathrm{ref}} = 0.8 \sin\left(\theta_{\mathrm{PLL}} - \frac{2\pi}{3}\right), \tag{3.67}$$

and

$$v_{c,\mathrm{ref}} = 0.8 \sin\left(\theta_{\mathrm{PLL}} + \frac{2\pi}{3}\right). \tag{3.68}$$

The coefficient 0.8 in Equations(3.66)-(3.68) represents the modulation index selected for the converter reference signals. It should not be interpreted as the physical magnitude of the PCC voltage. The reference signals supplied to the converter modulation stage are normalized quantities; therefore, the value 0.8 defines the amplitude of the modulation reference rather than the actual AC terminal voltage. For the initial synchronization study, this value was chosen to keep the generated converter references within the linear modulation region and to avoid overmodulation.

For easier interpretation of the PLL response during simulation, the estimated angular frequency is also converted from radians per second to hertz using Equation(3.69):

$$f_{\mathrm{PLL}} = \frac{\omega_{\mathrm{PLL}}}{2\pi}. \tag{3.69}$$

The overall signal flow of the implemented synchronization system can therefore be summarized as

$$\boxed{v_{abc,\mathrm{PCC}} \rightarrow v_{\alpha\beta} \rightarrow v_{dq} \rightarrow e_{\mathrm{PLL}} \rightarrow \Delta\omega \rightarrow \omega_{\mathrm{PLL}} \rightarrow \theta_{\mathrm{PLL}}} \tag{3.70}$$

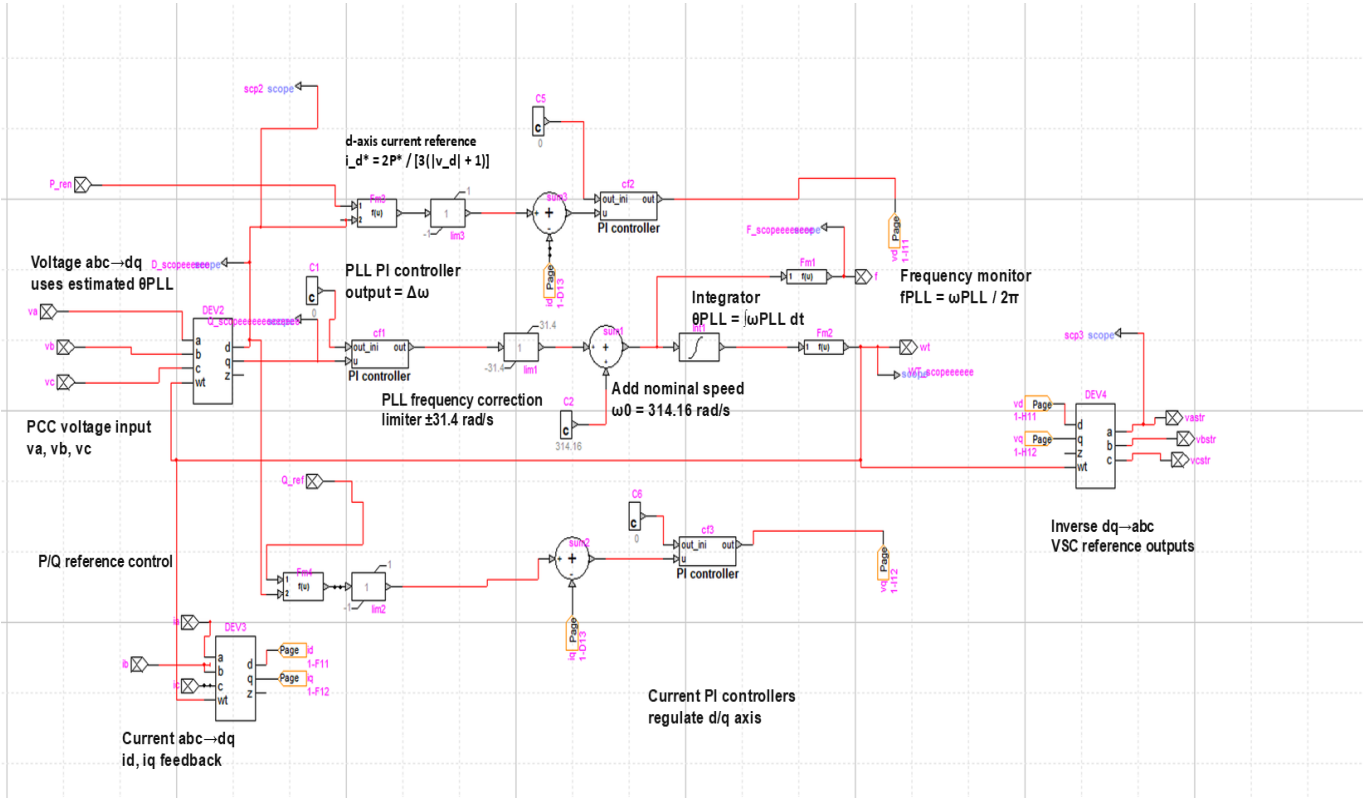


Figure 3.8: PLL control implementation in EMTP.

The complete PLL control arrangement implemented in EMTP is presented in Figure 3.3. The three-phase PCC voltages are passed through the reference-frame transformation blocks, after which the v_q component is compared with a zero reference. The resulting error is processed by the PI controller. Its output is limited between -31.4 and $+31.4$ rad/s, and the nominal angular frequency of 314.16 rad/s is subsequently added. The resulting ω_{PLL} is integrated to obtain θ_{PLL}. Finally, this estimated angle is fed back to the transformation block and is also used to generate the synchronized three-phase converter reference signals.

During the simulation, the main quantities used to evaluate PLL operation are v_d, v_q, θ_{PLL}, ω_{PLL}, and f_{PLL}. When stable synchronization has been achieved, v_q is expected to remain close to zero, v_d should remain close to the PCC voltage magnitude in per-unit form, and f_{PLL} should remain close to the nominal frequency of 50 Hz. Together, these signals provide an indication that the grid-following converter has successfully synchronized with the voltage established at the PCC.

The PLL therefore acts as the synchronization mechanism of the grid-following converter rather than as the source of the islanded system voltage or frequency. The grid-forming converter remains responsible for establishing the electrical conditions of the islanded AC network, while the grid-following converter observes these conditions through the PLL and adjusts its internal reference frame accordingly. In this way, the GFL converter can remain synchronized with the AC bus formed by the GFM converter without taking over the voltage- or frequency-forming function.

3.6.2 PLL-Based Grid-Following Converter Test Setup

The EMTPWorks model used to evaluate the grid-following converter with PLL-based synchronization is shown in Figure 3.9. The purpose of this model is to study how the converter follows an existing AC network voltage and generates synchronized converter reference signals. Unlike the grid-forming converter, the grid-following converter does not establish the AC voltage and frequency by itself. Instead, it measures the voltage at the point of common coupling (PCC) and uses a phase-locked loop (PLL) to synchronize with the existing AC system.
In the presented model, a stiff AC source is connected to the AC network. This source provides the initial voltage and frequency reference for the system. Since the converter is operated in grid-following mode, the stiff source acts as the main voltage-forming element, while the converter follows the voltage angle and frequency already present at the PCC. The green network lines in the figure represent the AC-side electrical connection between the stiff source, local load, converter output, and PCC.
A three-phase PQ load is connected to the AC bus. In this test case, the load is defined with an active-power demand of

$$P_{\text{load}} = 20 \text{ kW}, \tag{3.71}$$

and the reactive-power demand is set to

$$Q_{\text{load}} = 0 \text{ kVAr}. \tag{3.72}$$

This represents an approximately unity-power-factor load. The simplified load condition allows the synchronization behaviour and active-power response of the grid-following converter to be observed more clearly.
The converter is represented using an average-value converter model, labelled as the AVM converter in the figure. The average-value model represents the main electrical behaviour of the voltage-source converter without explicitly modelling the individual semiconductor switching events. This reduces the simulation complexity and is suitable for analysing the control response, synchronization behaviour, and power exchange at the PCC. The DC side of the converter is supplied by a DC source and capacitor arrangement, while the AC side is connected to the network through an RL filter.
The RL filter is placed between the converter output and the AC network. Its purpose is to smooth the converter output current and reduce high-frequency components before the converter is connected to the PCC. The filtered converter output is then connected to the same AC network where the stiff source and load are present. The PCC is located on the right side of the model. Voltage and current measurement blocks are connected at this point. The measured PCC voltages are used as the main input signals for the PLL control block. These three-phase voltages can be expressed as shown in Equation (3.73):

$$v_{abc,\text{PCC}} = \begin{bmatrix} v_a \\ v_b \\ v_c \end{bmatrix}. \tag{3.73}$$

The measured PCC voltage is supplied to the PLL control block, where the phase angle and frequency of the existing AC network are estimated. The PLL does not create a new voltage reference for the network. Instead, it extracts the synchronization angle from the PCC voltage so that the converter can align its internal reference frame with the AC bus.
Inside the block labelled PLL Control, the measured three-phase voltages, converter current signals, active-power reference, and reactive-power reference are processed. The PCC voltage signals are used by the PLL to estimate the electrical angle and frequency. The current and power signals are used for the grid-following converter control, allowing the converter to inject power while remaining synchronized with the PCC voltage.
The main synchronization path can be written as

$$v_{abc,\mathrm{PCC}} \rightarrow \mathrm{PLL} \rightarrow \theta_{\mathrm{PLL}},\ f_{\mathrm{PLL}}. \tag{3.74}$$

Here, θ_{PLL} is the estimated voltage angle, and f_{PLL} is the estimated system frequency. These signals are then used to generate the three-phase voltage-reference signals for the converter.
The output reference signals from the PLL control block are

$$v_{a,\mathrm{ref}}, \qquad v_{b,\mathrm{ref}}, \qquad v_{c,\mathrm{ref}}. \tag{3.75}$$

These signals are connected to the V_{ref} input of the average-value converter. Therefore, the converter output is controlled according to the reference waveforms generated by the PLL-based control block. The general reference-generation path can be summarized as

$$\theta_{\mathrm{PLL}} \rightarrow v_{abc,\mathrm{ref}} \rightarrow V_{\mathrm{ref}} \rightarrow \text{AVM converter}. \tag{3.76}$$

The PLL control block also provides monitoring outputs such as the estimated frequency f_{PLL} and the electrical angle ωt. These signals are useful for verifying that the converter remains synchronized with the AC network. Under correct grid-following operation, the estimated frequency should remain close to the nominal system frequency, and the generated three-phase reference signals should remain balanced and synchronized with the PCC voltage.
A switching arrangement is also included near the PCC. This allows different operating conditions to be tested by connecting or disconnecting parts of the AC network. During the initial condition, the stiff AC source establishes the voltage and frequency at the PCC. The grid-following converter then measures this voltage, locks onto it through the PLL, and produces synchronized reference signals for the AVM converter.
The key point in this implementation is that the converter is operated as a grid-following unit. It does not independently form the PCC voltage or frequency. Instead, it follows the voltage angle and frequency imposed by the stiff AC source or by another voltage-forming unit in the network. The PLL is therefore the main synchronization mechanism that allows the converter to align its reference signals with the existing AC bus.

This control arrangement is different from the grid-forming converter control used in the islanded test case. In the grid-forming converter, the controller internally generates the voltage magnitude, frequency, and phase angle required to establish the AC network. In contrast, the grid-following converter depends on the measured PCC voltage and uses the PLL to obtain the required synchronization angle. This distinction is important because the grid-following converter can inject controlled power into the network, but it cannot act as the main voltage-forming source without an additional grid-forming control structure.
The main quantities monitored in this test setup include the PCC voltage, converter current, active and reactive power, PLL frequency, PLL angle, and the three-phase voltage-reference signals supplied to the AVM converter. These signals are used to confirm that the converter remains synchronized with the AC network and that the generated reference signals are correctly aligned with the PCC voltage.

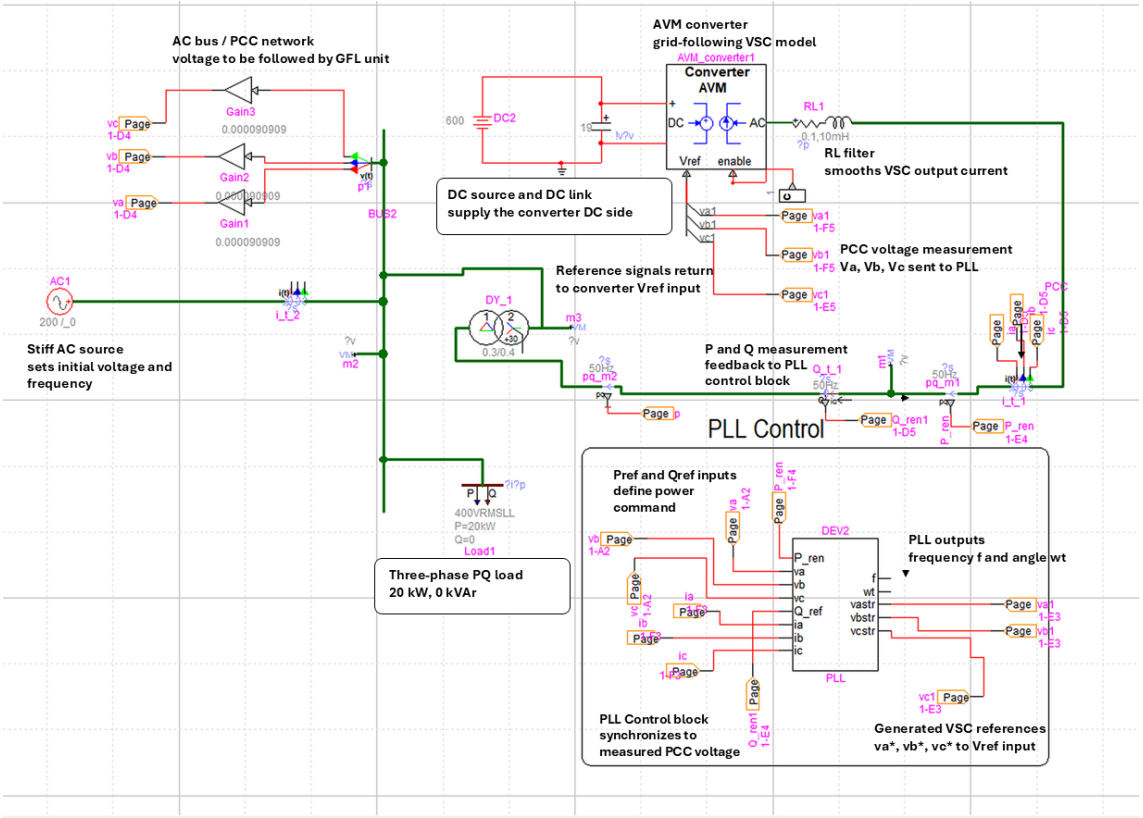


Figure 3.9: EMTPWorks test setup for the PLL-based grid-following converter.

4

Results

4.1 Battery Charging During Surplus Condition

From Figure 4.1, The first case considers the battery operation when the initial battery state of charge (SOC) is set to 50%. At the beginning of the simulation, the wind turbine output, P_{wind} (yellow curve), increases gradually due to the estimated wind speed profile and the turbine dynamic response. The simulated wind power reaches approximately 20–21 kW around 150 s. Before this point, the renewable generation is not sufficient to fully support the load demand. Therefore, the battery power, P_{bat} (green curve), shows a discharge of approximately 6.5 kW to support the islanded grid.

After 150 s, the wind turbine reaches a more stable operating region and produces around 20 kW. During this instant, the load demand, P_{load} (purple curve), is relatively low, around 5 kW, while the solar power contribution, P_{solar} (red curve), is almost 0 kW due to low irradiance or cloudy conditions. Since the wind generation alone is higher than the load demand, a surplus power condition occurs. As a result, the controller generates a negative battery power reference of approximately -15 kW. The negative value indicates that the battery is charging by absorbing the excess renewable power.

A clearer surplus condition can be observed between 500 s and 600 s. During this period, the wind power is approximately 21 kW and the solar power is around 0.5 kW. Therefore, the total renewable generation is calculated as Equation(4.1):

$$P_{\text{ren}} = P_{\text{wind}} + P_{\text{solar}} \tag{4.1}$$

$$P_{\text{ren}} = 21 + 0.5 = 21.5 \text{ kW} \tag{4.2}$$

During the same interval, the load demand is lower than the renewable generation. From the simulation result, the controller produces a battery reference of approximately:

$$P_{\text{batt,ref}} = -8.2 \text{ kW} \tag{4.3}$$

The negative sign confirms that the battery is charging. Since $P_{\text{ren}} > P_{\text{load}}$ and the battery SOC is around 50%, the controller allows the surplus renewable power to charge the battery. Therefore, the surplus condition of the power balance controller is operating as expected.

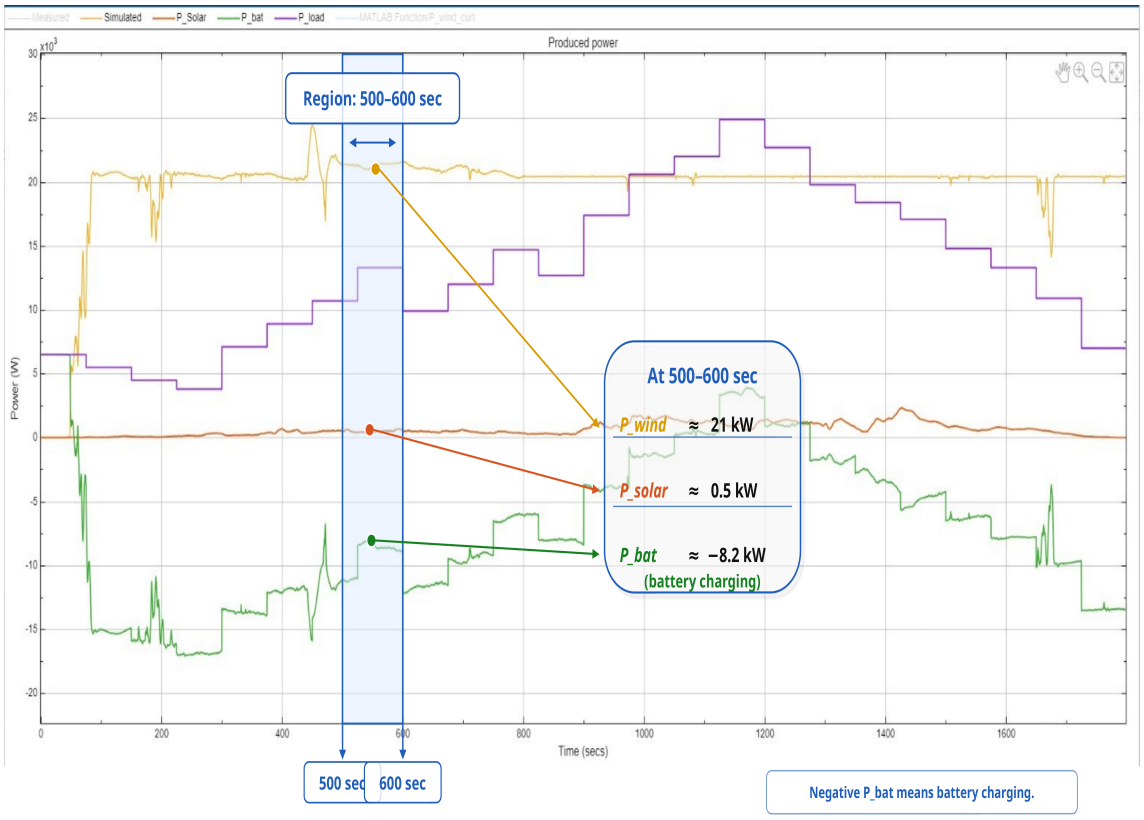


Figure 4.1: Power balance controller response during surplus.

4.2 Battery Discharging During Deficit Condition

The deficit condition is analysed between 1100 s and 1200 s, as shown in Figure 4.2. During this interval, the load demand, P_{load}, is approximately 24.8 kW, while the combined wind and solar generation, $P_{\text{wind}} + P_{\text{solar}}$, is around 21.6 kW. Therefore, the renewable generation is not sufficient to supply the full load demand.
The battery reference power is calculated as Equation(4.4):

$$P_{\text{batt,ref}} = P_{\text{load}} - P_{\text{ren}} \tag{4.4}$$

$$P_{\text{batt,ref}} = 24.8 - 21.6 = 3.2 \text{ kW} \tag{4.5}$$

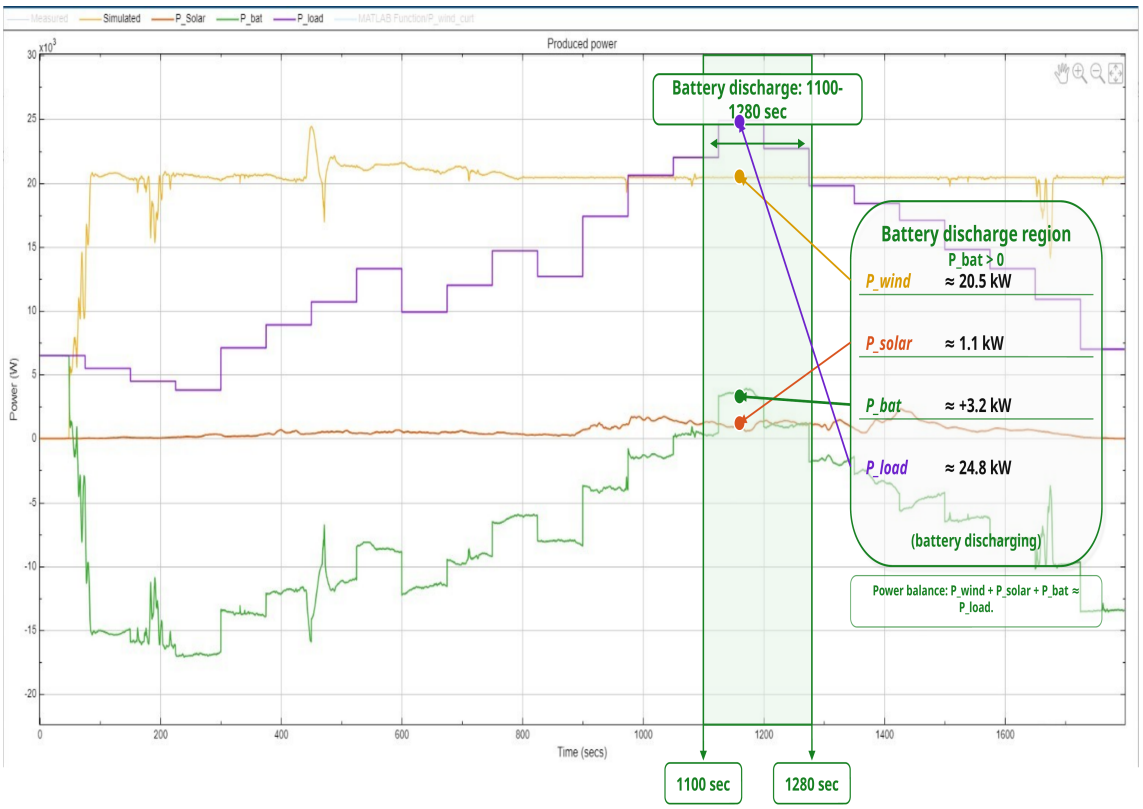


Figure 4.2: Power balance controller response during deficit.

In this case, the controller generates a positive battery reference of approximately 3.2 kW. The positive value indicates that the battery is discharging and supplying power to the grid. Since $P_{\text{load}} > P_{\text{ren}}$ and the battery SOC is above the minimum SOC limit, the battery supports the system by covering the power deficit. This confirms that the deficit condition of the controller is operating properly.

4.3 Curtailment Operation During Full Battery Condition

The curtailment logic is analysed using the same surplus period between 500 s and 600 s, as shown in Figure 4.3. In this case, the initial battery SOC is set to 100%. Therefore, the battery is fully charged and cannot absorb additional surplus renewable power.

During this period, the wind turbine power, P_{wind}, is approximately 21 kW, while the solar power, P_{solar}, is around 0.5 kW. Therefore, the total renewable generation is approximately 21.5 kW. The load demand, P_{load}, is around 13.3 kW. Since the renewable generation is higher than the load demand and the battery is already fully charged, the controller cannot transfer the excess power to the battery. Therefore, the surplus power must be curtailed to maintain the power balance in the islanded system.

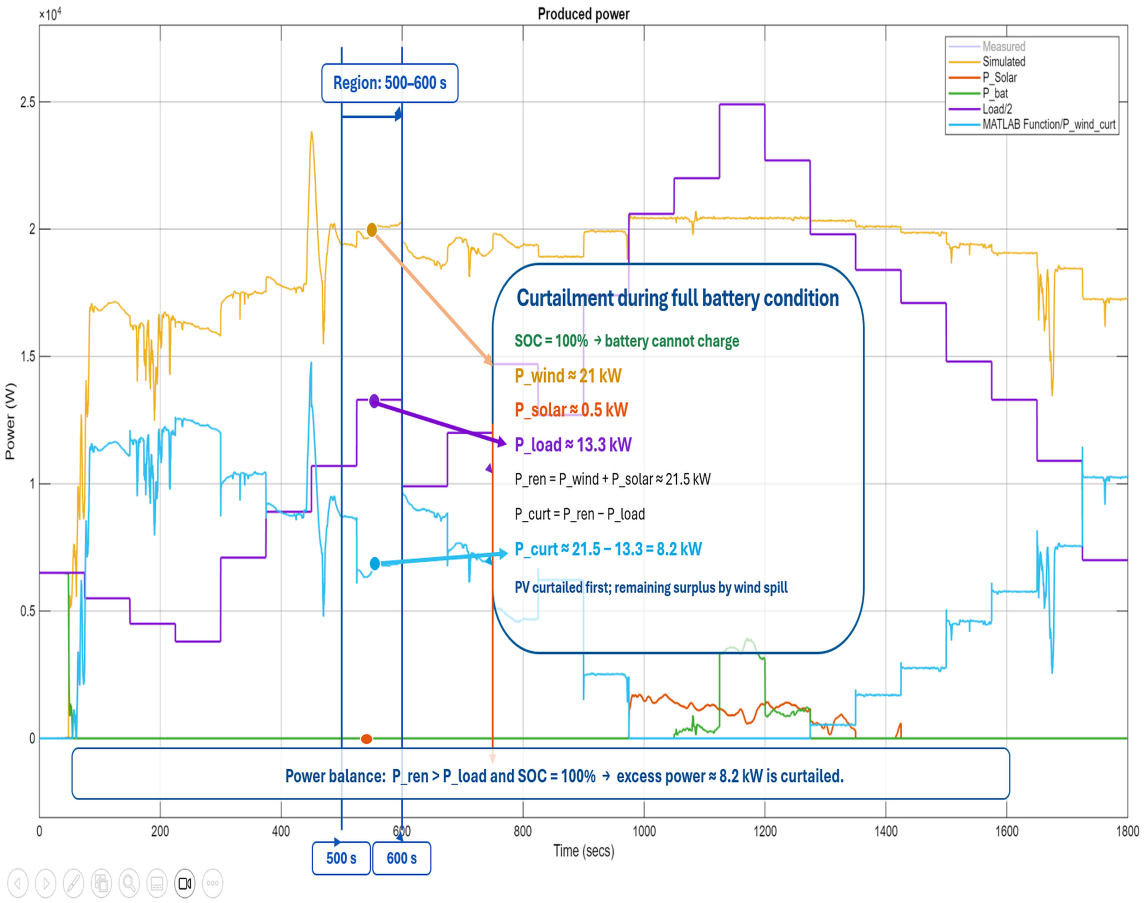


Figure 4.3: Curtailment response during surplus renewable generation with 100% battery SOC.

The required curtailment power is calculated as shown in Equations (4.6) and (4.7)

$$P_{\text{curt}} = P_{\text{ren}} - P_{\text{load}} \tag{4.6}$$

$$P_{\text{curt}} = 21.5 - 13.3 = 8.2 \text{ kW} \tag{4.7}$$

From the simulation result, the curtailment signal, P_{curt}, operates around 8.2 kW, which matches the excess power that must be removed from the system. The controller logic is arranged so that the PV generation is curtailed first. This follows the Björkö control approach, where solar generation is switched off before wind power reduction is applied. After the PV power is curtailed, the remaining surplus power is reduced by wind spilling.
As a result, the effective wind power output decreases and follows the load demand more closely. Therefore, the curtailment logic works as expected under the condition where $P_{\text{ren}} > P_{\text{load}}$ and the battery SOC is at its maximum limit.

4.4 Load Shedding During Empty Battery Condition

The load shedding logic is analysed using the same deficit period between 1100 s and 1200 s, as shown in Figure 4.4. In this case, the initial battery SOC is set to 0%. Therefore, the battery is empty and cannot discharge power to support the load demand.
During this period, the load demand, P_{load}, is initially around 25 kW, while the available renewable generation from wind and solar is lower than the load demand. This deficit condition is expressed in Equation (4.8).

$$P_{\text{load}} > P_{\text{ren}} \tag{4.8}$$

Since the battery SOC is at its minimum limit, the battery cannot supply the missing power. Therefore, the controller activates the load shedding logic to reduce the load demand according to the available renewable generation.
From the simulation result, the load is reduced from approximately 25 kW to around 21.6 kW. At the same time, the combined wind and solar generation is also approximately 21.6 kW. This means that after load shedding, the load demand becomes nearly equal to the available renewable power,as shown in Equation (4.9)

$$P_{\text{load,after shedding}} \approx P_{\text{wind}} + P_{\text{solar}} \tag{4.9}$$

$$P_{\text{load,after shedding}} \approx 21.6 \text{ kW} \tag{4.10}$$

This behaviour is expected because the purpose of load shedding is to remove the unmet portion of the load when neither renewable generation nor the battery can supply it. Therefore, after shedding the excess load demand, the system reaches a balanced operating condition where the generated power matches the remaining load.
This confirms that the load shedding logic operates correctly under the condition where $P_{\text{load}} > P_{\text{ren}}$ and the battery SOC is too low to support the deficit.

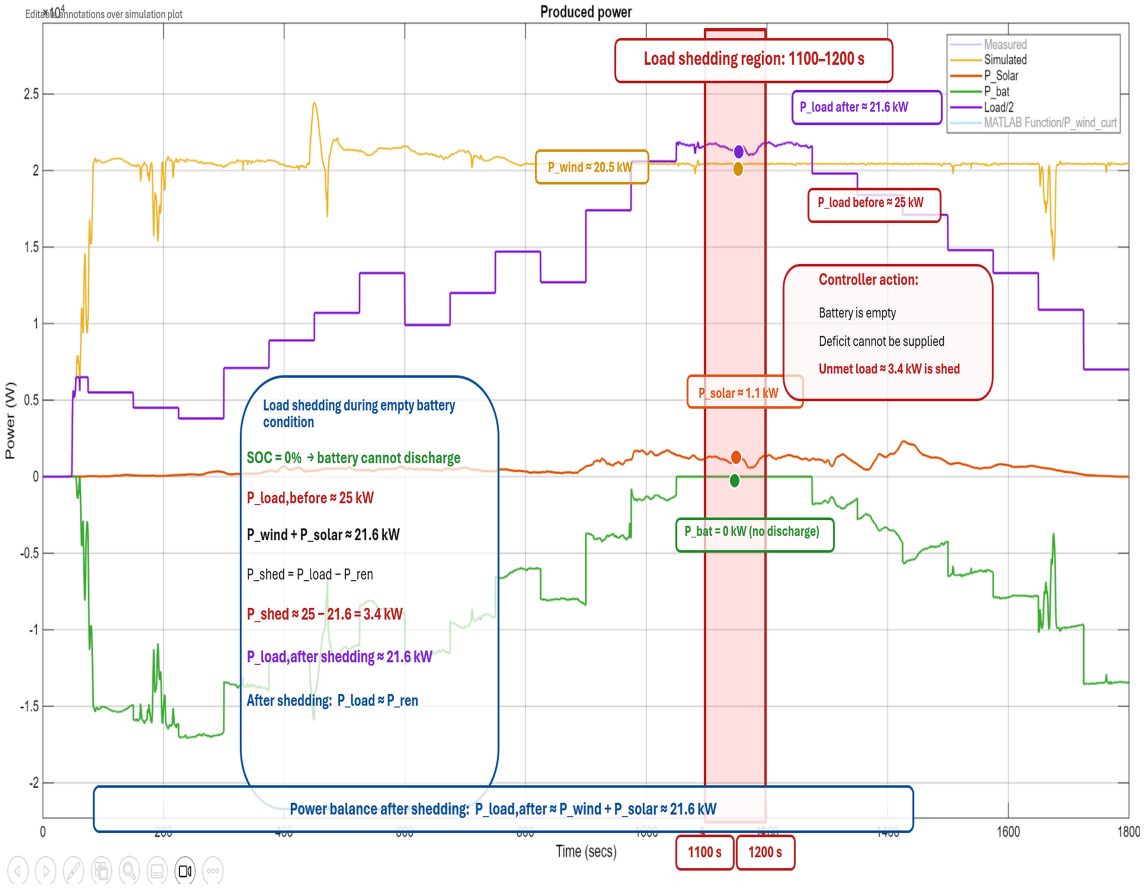


Figure 4.4: Load shedding response.

4.5 Result Discussion for the GFM-Based Islanded Case

The PCC voltage reference was set to 400 $V_{LL,rms}$. For a balanced three-phase system, this corresponds to a phase RMS voltage is calculated using Equation (4.11)

$$V_{ph,rms} = \frac{400}{\sqrt{3}} \approx 230.9 \text{ V} \tag{4.11}$$

The corresponding phase peak voltage is calculated using Equation (4.12)

$$V_{ph,peak} = \sqrt{2} \times 230.9 \approx 326.6 \text{ V} \tag{4.12}$$

Therefore, when the converter is maintaining the nominal AC voltage, the phase voltage waveform at the PCC is expected to remain close to ±326 V.
The simulation was carried out for 2 s. During the initial part of the simulation, the PCC voltage and frequency were supported by the stiff AC source. At approximately $t = 0.3$ s, the switching elements disconnected the stiff AC source from the PCC. This created the islanded operating condition and forced the battery-fed GFM converter to take over the voltage-forming role.

Immediately after the disconnection, a short voltage transient can be observed. This response is expected because the external voltage source is removed and the converter must establish the PCC voltage using its own control reference. After this brief transition period, the voltage waveform is restored and remains sinusoidal with a phase peak value close to 326 V. This corresponds to the intended 400 $V_{LL,rms}$ operating point and shows that the voltage-reference loop is able to regulate the PCC voltage after islanding.

After the transient period, about ten complete voltage cycles can be observed within a 0.2 s interval. The frequency can therefore be estimated as Equation(4.13):

$$f = \frac{N}{\Delta t} \tag{4.13}$$

$$f = \frac{10}{0.2} = 50 \text{ Hz} \tag{4.14}$$

This suggests that the GFM converter maintains the PCC frequency close to the nominal value of 50 Hz after the stiff AC source is disconnected. The battery SOC shows a slight decreasing trend during the islanded period. This indicates that the battery is discharging and supplying power to the local load. Since the tested case represents a deficit condition, where the available generation is not sufficient to meet the load demand, the battery-fed converter provides the required active-power support after the stiff AC source is removed.

Overall, the result demonstrates the basic grid-forming behaviour of the developed controller for the tested deficit-based islanded case. After the external source is disconnected, the battery-fed converter restores and maintains the PCC voltage close to 400 $V_{LL,rms}$, while the waveform indicates operation close to 50 Hz. The decreasing SOC further confirms that the battery is actively supporting the islanded load. Therefore, for this specific test condition, the converter is able to operate as the voltage- and frequency-forming unit at the PCC.

Since only one islanded condition was tested, this result should be interpreted as a validation of the basic GFM functionality for the selected case, rather than a complete validation of the controller under all possible operating conditions.

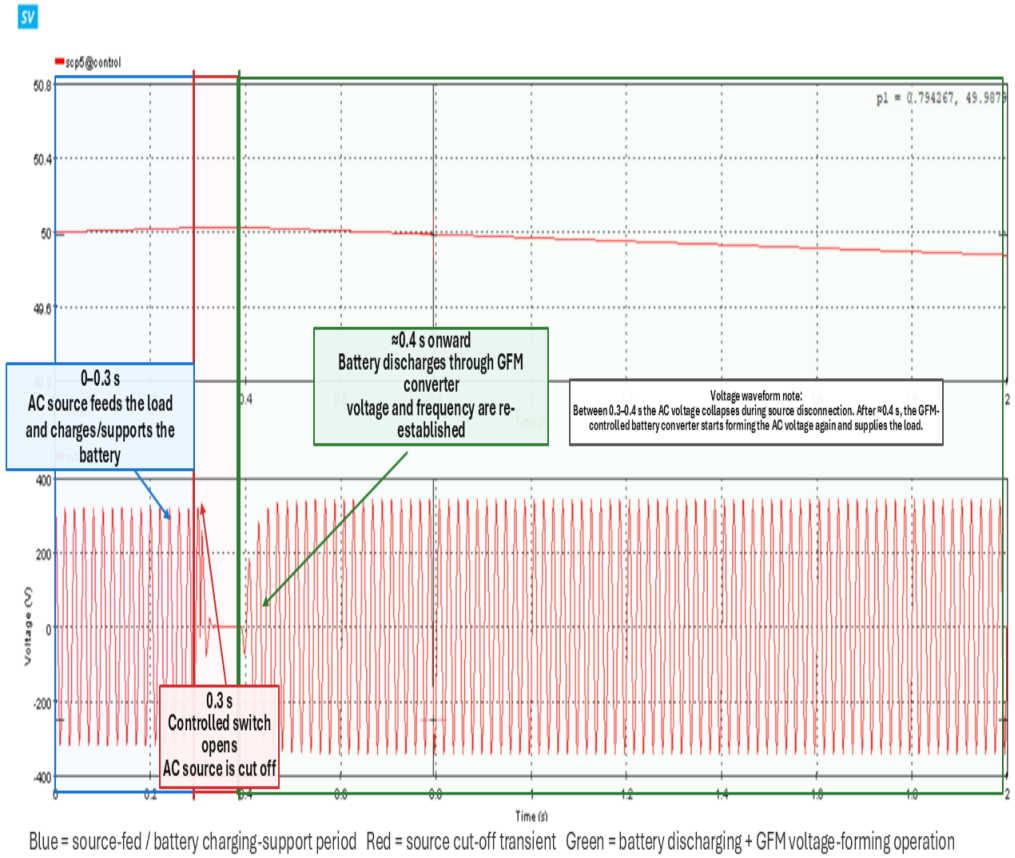


Figure 4.5: GFM behaviour at the PCC.

4.6 Verification of Grid-Following Converter Synchronization

The grid-following (GFL) converter was initially tested using a stiff three-phase AC source in EMTP to examine the synchronization performance of the phase-locked loop (PLL) controller. The stiff AC source provides a stable voltage and frequency reference, allowing the PLL response to be evaluated before considering its operation in the complete islanded power system.
In the simulation, the three-phase voltages measured at the point of common coupling (PCC) were supplied to the PLL controller. Based on these measurements, the PLL estimates the phase angle and frequency of the AC source. The estimated phase angle is then used as the synchronization reference for the converter. To verify the PLL operation, the PCC voltage waveform was first examined, followed by the internal q-axis voltage and frequency responses.

4.6.1 PCC Voltage Waveform

Figure 4.6 presents the PCC voltage waveform obtained during the simulation with the stiff AC source connected. The waveform remains sinusoidal over the 0.5-second

simulation period, with a nearly constant amplitude and a frequency of approximately 50 Hz. No significant voltage fluctuations or sustained oscillations are observed.
The stiff AC source maintains the PCC voltage and provides the reference required for synchronization. The PLL uses the measured voltage to estimate the phase angle and frequency of the AC system. The steady sinusoidal waveform indicates that a stable voltage reference is available for the controller.
However, the PCC voltage waveform alone does not confirm that the PLL has achieved synchronization. Therefore, the internal PLL signals were also examined to verify whether the controller was correctly tracking the AC source.

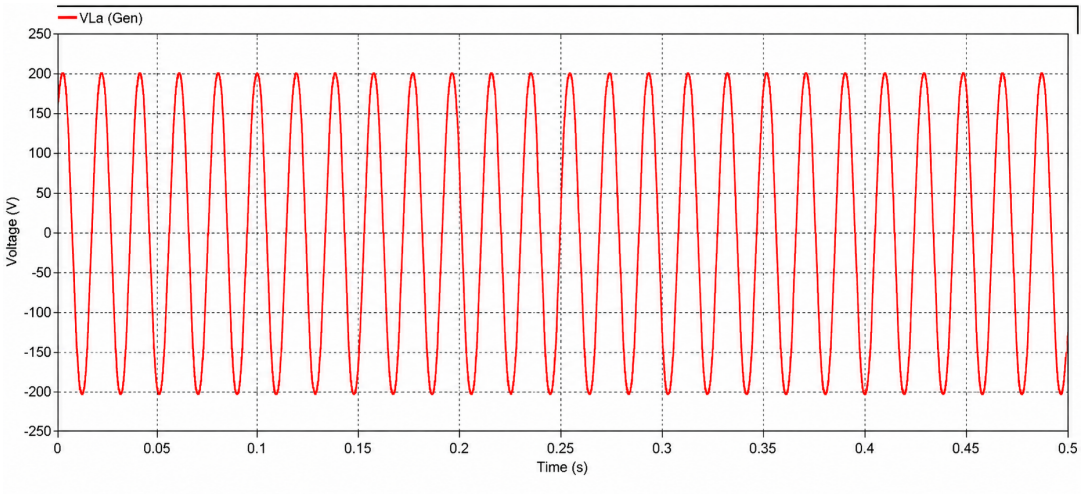


Figure 4.6: PCC voltage waveform during the PLL synchronization test with a stiff three-phase AC source.

4.6.2 Verification of PLL Performance

The synchronization performance of the PLL was evaluated by observing the q-axis voltage (V_q) and the estimated frequency. These two signals provide an indication of how the controller responds during the synchronization process.
The PLL transforms the measured three-phase PCC voltages into the rotating dq reference frame. During synchronization, the controller adjusts its estimated phase angle to align the d-axis with the AC voltage vector. When the reference frame is aligned, the q-axis voltage approaches zero.
The upper plot in Figure 4.7 shows the q-axis voltage response. At the beginning of the simulation, a short transient occurs as the PLL adjusts its initial phase-angle estimate to match the AC source. During this period, small oscillations are observed before the q-axis voltage gradually decreases toward zero. After approximately 0.2 seconds, the oscillations have almost disappeared, and the q-axis voltage remains close to zero for the remainder of the simulation.
The lower plot in Figure 4.7 presents the frequency estimated by the PLL. Small deviations from the nominal frequency can be observed during the initial synchronization period. However, these variations decrease rapidly, and the estimated fre-

quency settles at approximately 50 Hz, remaining stable throughout the rest of the simulation.
The responses of the q-axis voltage and estimated frequency indicate that the PLL successfully synchronizes with the stiff AC source. The q-axis voltage approaching zero indicates alignment of the rotating reference frame with the PCC voltage vector, while the stable frequency confirms that the controller is tracking the 50 Hz source.

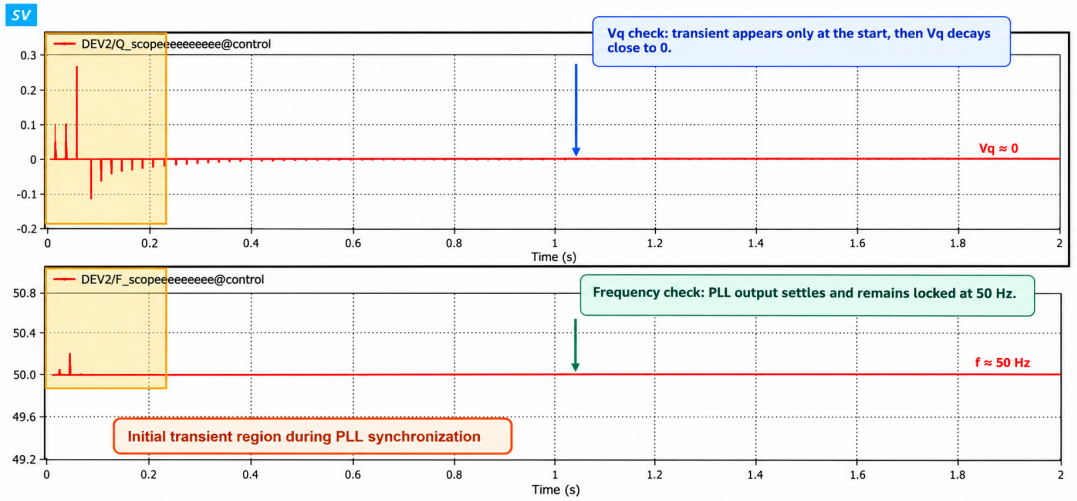


Figure 4.7: PLL synchronization verification showing the q-axis voltage and estimated frequency during operation with a stiff AC source.

The results confirm that the implemented PLL is able to establish and maintain synchronization with the stiff AC source under the tested conditions. This verifies the synchronization stage of the grid-following converter control system and provides a basis for its subsequent integration with the islanded power system. The test does not independently verify active or reactive power regulation by the converter.

5

Conclusion

This thesis investigated the power management and control of an islanded power system consisting of wind generation, solar photovoltaic (PV) generation, and battery energy storage. The main objective was to examine how these energy sources could be coordinated to maintain the balance between power generation and load demand when operating independently of the main grid. MATLAB/Simulink was used to develop and evaluate the renewable generation models and energy management strategy, while EMTP was used to investigate the electrical behaviour of the GFM and GFL converter control structures.

The developed energy management system (EMS) was designed to coordinate the available renewable generation, battery operation, and load demand. The control strategy prioritised the use of wind and solar power, with the battery providing additional support whenever there was a difference between generation and consumption. The simulation results demonstrated that the controller responded to the different operating conditions according to the implemented power balance logic.

During surplus generation, the battery absorbed the excess renewable power. For the operating period between 500 and 600 seconds, the total renewable generation was approximately 21.5 kW, and the controller generated a negative battery power reference of around 8.2 kW, indicating charging operation. In contrast, during the deficit condition, the load demand increased to approximately 24.8 kW while the available renewable generation was around 21.6 kW. The resulting power shortage of 3.2 kW was supplied by the battery through a positive power reference. These results showed that the controller could determine the required battery operating mode based on the available generation and load demand.

The energy management strategy was also evaluated under conditions where the battery could no longer provide charging or discharging support. When the battery was fully charged, the controller activated renewable power curtailment to reduce the surplus generation. In the simulated case, approximately 8.2 kW of excess power was curtailed, with solar PV generation reduced first, followed by wind power when further reduction was required. Similarly, when the battery was considered empty during a power deficit, load shedding was activated to reduce the demand according to the available renewable generation. The load was reduced from approximately 25 kW to 21.6 kW, bringing the demand close to the available generation. These results demonstrated that the developed controller could respond to the battery operating limits by adjusting renewable generation or load demand when battery support was unavailable.

In addition to the power management strategy, the converter control structures were investigated to understand their roles in islanded operation. The battery-supported

GFM converter was developed to establish the voltage and frequency reference at the point of common coupling (PCC). In the EMTP simulation, the system was initially connected to a stiff AC source, which provided the voltage and frequency reference during the starting period. At approximately 0.3 seconds, the external source was disconnected, requiring the GFM converter to support the local AC network independently.

Following disconnection, a short voltage transient was observed before the PCC voltage returned to a stable sinusoidal waveform. The phase-voltage peak was close to 326 V, corresponding to the intended 400 V line-to-line RMS system voltage. The waveform also indicated a frequency close to 50 Hz after islanding. In addition, the decreasing battery state of charge suggested that the battery was discharging to support the connected load. These observations showed that the developed GFM controller could maintain the basic voltage- and frequency-forming functions for the selected islanded operating condition.

The GFL converter was investigated separately using a phase-locked loop (PLL) controller. Unlike the GFM converter, the GFL converter requires an existing AC voltage reference to estimate the phase angle and frequency of the network. For this verification, the PLL-controlled converter was tested against a stiff three-phase AC source. The PCC voltage remained sinusoidal and provided a stable reference for the PLL. The internal controller responses were then examined using the q-axis voltage and estimated frequency. The q-axis voltage showed a short initial transient before approaching zero within approximately 0.2 seconds, while the estimated frequency converged to 50 Hz and remained stable. These observations confirmed that the PLL could synchronize with the applied AC source under the tested conditions.

The intended arrangement was to operate the GFM and GFL converters together within the same islanded network. In this configuration, the GFM converter would establish the PCC voltage and frequency, while the GFL converter would use the PLL to synchronize with the voltage already present in the network. However, difficulties were encountered when connecting the two converter systems in the EMTP model. Although the individual controllers demonstrated the expected behaviour during their respective tests, the combined arrangement resulted in a reduction in the PCC voltage magnitude, preventing stable operation of the integrated system.

Based on the observed behaviour, the voltage reduction was considered possibly related to differences in the dynamic responses of the two control systems. A mismatch in controller parameters or response bandwidths could affect the phase alignment between the voltage generated by the GFM converter and the reference followed by the GFL converter. This could contribute to an unwanted interaction between the converters and the resulting reduction in PCC voltage. However, detailed controller tuning, bandwidth coordination, and investigation of these interactions were outside the defined scope of the thesis. Therefore, the exact cause of the observed voltage reduction was not established.

Due to this limitation, the individual converter control structures were evaluated using separate simulation arrangements. The GFM controller was examined by disconnecting the stiff AC source and observing whether the converter could maintain the local voltage and frequency. The GFL controller was tested against a continuously connected stiff AC source to verify its PLL synchronization performance.

These tests provided useful information about the individual functions of the two converter control structures, although they did not establish successful coordinated operation when both converters were connected to the same islanded network.
The findings should therefore be understood within the limitations of the simulations carried out. The MATLAB/Simulink results demonstrated the intended operation of the power management strategy under the selected surplus, deficit, curtailment, and load-shedding conditions. The EMTP simulations verified the basic voltage- and frequency-forming behaviour of the GFM converter and the synchronization capability of the GFL PLL. However, complete integration of the two converters and validation of their coordinated operation remained unresolved. Addressing this would require a separate investigation of controller interactions and coordination, which was beyond the scope of the present work.
Overall, the thesis demonstrates how a rule-based power management strategy can coordinate wind generation, solar PV, and battery storage to respond to changing generation and load conditions in an islanded system. The simulation results showed that the developed EMS could determine the required battery power and apply renewable curtailment or load shedding when the battery was unable to provide further support. The converter simulations also demonstrated the individual roles of GFM voltage and frequency regulation and GFL synchronization. At the same time, the difficulties encountered during converter integration highlighted that satisfactory performance in separate tests does not necessarily ensure stable operation when multiple converters are connected together. The study therefore establishes a basis for further investigation of the complete islanded system, where both power balance and coordinated converter operation are necessary to achieve the intended system performance.

Bibliography

[1] International Renewable Energy Agency (IRENA), Renewable Capacity Statistics 2026. Abu Dhabi, United Arab Emirates: IRENA, Mar. 2026. [Online]. Available: https://www.irena.org/-/media/Files/IRENA/Agency/Publication/2026/Mar/IRENA_DAT_RE_capacity_statistics_2026.pdf

[2] Zhao, Yujie. (2025). A Review of Renewable Energy and Power System Integration. Applied and Computational Engineering. 126. 10-15. 10.54254/2755-2721/2025.20092.

[3] Md Akib Hasan a, Md Showkot Hossain b, Mohd Azrik Roslan a, Azralmukmin Azmi a, Leong Jenn Hwai a, Ahmad Afif Nazib a, Noor Syafawati Ahmad a. (2025) A comprehensive review of control strategies and efficiency optimization for islanded AC microgrids IFAC Journal of Systems and Control,Volume 33.

[4] Patwary, A., Sayem, M., Hossain, M., Halim, M. (2024), A Review of Energy Storage Systems (ESS) for Integrating Renewable Energies in Microgrid. J.Control Systems and Optimization Letters. https://ejournal.csol.or.id/index.php/csol/article/view/6.

[5] Mir Nahidul Ambia, Ahmed Al-Durra, Cedric Caruana, S.M. Muyeen,(2016) Islanding operation of hybrid microgrids with high integration of wind driven cage induction generators,Sustainable Energy Technologies and Assessments,Volume 13,

[6] Bukhari, Syed Ahsan Iftikhar Mal, Aijaz (2024) Islanded Operation of Wind Turbine with Solar Power and Battery Storage https://hdl.handle.net/20.500.12380/308928.

[7] M. Eriksson, “Frekvensstyrning med vindkraft,” Tech. Rep. 2023:3, Dept. Elect. Eng., Div. Electr. Power Eng., Chalmers Univ. Technol., Gothenburg, Sweden, 2022.

[8] Alessandro Rosini, Renato Procopio, Andrea Bonfiglio, On the use of frequency in the primary control of fully inverter based islanded microgrids, International Journal of Electrical Power and Energy Systems, Volume 143, 2022,

[9] Mario Rizo, Marco Liserre, Emilio Bueno, Francisco J. Rodríguez, Francisco Huerta, Universal wind turbine working in grid-connected and island operating modes, Mathematics and Computers in Simulation, Volume 91, 2013,

[10] T.L. Vandoorn, J.D.M. De Kooning, B. Meersman, L. Vandevelde, Review of primary control strategies for islanded microgrids with power-electronic interfaces, Renewable and Sustainable Energy Reviews, Volume 19, 2013,

[11] D. Pagnani, L. Kocewiak, J. Hjerrild, F. Blaabjerg and C. L. Bak, "Control Principles for Island Operation and Black Start by Offshore Wind Farms inte-

grating Grid-Forming Converters," 2022 24th European Conference on Power Electronics and Applications (EPE'22 ECCE Europe), Hanover, Germany, 2022

[12] Md Ismail Hossain, Hasanur Zaman Anonto, Ahmed Intekhab Rohan, Abu Shufian, Debashish Kumar Ghosh.(2025)Optimizing power distribution and stability in islanded microgrids with wind energy integration using enhanced droop and virtual impedance control,Results in Engineering,Volume 27,

[13] Peña Asensio, A., Arnaltes Gómez, S., Rodriguez-Amenedo, J. L., García Plaza, M., Eloy-García Carrasco, J., Alonso-Martínez de las Morenas, J. M. (2018). A Voltage and Frequency Control Strategy for Stand-Alone Full Converter Wind Energy Conversion Systems. Energies, 11(3), 474. https://doi.org/10.3390/en11030474

[14] Belenguer, E ,Vidal-Albalate, Ricardo, Blasco-Gimenez, Ramon, Beltran, Hector, Alfonso, José, Ariño, Carlos. (2013). Islanded Operation and Control of Offshore Wind Farms Connected through a VSC-HVDC Link. Renewable Energy and Power Quality Journal. 11. 10.24084/repqj11.366.

[15] S. K. Chaudhary, R. Teodorescu, J. R. Svensson, Ł. H. Kocewiak, P. Johnson and B. Berggren, "Islanded Operation of Offshore Wind Power Plant using IBESS," 2021 IEEE Power, Energy Society General Meeting (PESGM), Washington, DC, USA, 2021, pp. 1-5, doi: 10.1109/PESGM46819.2021.9638226.

[16] Narula. Anant (2023) Grid-forming wind power plants, Department of Electrical Engineering Chalmers University of Technology

[17] S. Rajendran, M. Diaz, R. Cárdenas, E. Espina, E. Contreras, and J. Rodriguez, "A review of generators and power converters for multi-MW wind energy conversion systems," *Processes*, vol. 10, Art. no. 2302, Nov. 2022, doi: 10.3390/pr10112302.

[18] O. Alkul, D. Syed, and S. Demirbas, "A review of wind energy conversion systems," in *Proc. 10th IEEE International Conference on Smart Grid (icSmartGrid)*, Istanbul, Turkey, Jun. 27–29, 2022.

[19] O. C. Castillo, V. R. Andrade, J. J. Rodríguez Rivas, and R. O. González, "Comparison of power coefficients in wind turbines considering the tip speed ratio and blade pitch angle," *Energies*, vol. 16, Art. no. 2774, Mar. 2023, doi: 10.3390/en16062774.

[20] P. O. Ochieng, A. W. Manyonge, and A. O. Oduor, "Mathematical analysis of tip speed ratio of a wind turbine and its effects on power coefficient," *International Journal of Mathematics and Soft Computing*, vol. 4, no. 1, pp. 61–66, 2014.

[21] Å. Larsson, *The Power Quality of Wind Turbines*, Ph.D. dissertation, Dept. Electric Power Engineering, Chalmers University of Technology, Göteborg, Sweden, 2000.

[22] N. Ramesh Babu and P. Arulmozhivarman, "Wind energy conversion systems—A technical review," *Journal of Engineering Science and Technology*, vol. 8, no. 4, pp. 493–507, Aug. 2013.

[23] Christian Bipongo Ndeke, Marco Adonis, Ali Almaktoof. (2024). Energy management strategy for a hybrid micro-grid system using renewable energy. Discover Energy, Volume 4, Article 1. https://doi.org/10.1007/s43937-024-00025-9.

[24] Imene Yahyaoui, Natalia Vidal de la Peña. (2022). Energy Management Strategy for an Autonomous Hybrid Power Plant Destined to Supply Controllable Loads. Sensors, Volume 22, Article 357. https://doi.org/10.3390/s22010357.

[25] Rona George Allwyn, Amer Al-Hinai, Vijaya Margaret. (2023). A comprehensive review on energy management strategy of microgrids. Energy Reports, Volume 9, 5565–5591. https://doi.org/10.1016/j.egyr.2023.04.360.

[26] Süleyman Emre Eyimaya, Necmi Altin. (2024). Review of Energy Management Systems in Microgrids. Applied Sciences, Volume 14, Article 1249. https://doi.org/10.3390/app14031249.

[27] P. Satish Kumar, R.P.S. Chandrasena, V. Ramu, G.N. Sreenivas, K. Victor Sam Moses Babu. (2020). Energy Management System for Small Scale Hybrid Wind Solar Battery Based Microgrid. IEEE Access. https://doi.org/10.1109/ACCESS.2020.2964052.

[28] Mahmoud Elkazaz, Mark Sumner, David Thomas. (2020). Energy management system for hybrid PV-wind-battery microgrid using convex programming, model predictive and rolling horizon predictive control with experimental validation. International Journal of Electrical Power and Energy Systems, Volume 115, 105483. https://doi.org/10.1016/j.ijepes.2019.105483.

[29] EMTP, "EMTP® Overview," *EMTP Documentation*. [Online]. Accessed: Aug. 7, 2026.

[30] H. Ashourian and H. Gras, "Three-phase grid-connected converter," *EMTP–EMTPWorks Documentation*, 2021. [Online]. Accessed: Aug. 7, 2026.

[31] EMTP, "Renewable energy systems," *EMTP Applications*. [Online]. Accessed: Aug. 7, 2026.

[32] A. V. Timbus, R. Teodorescu, F. Blaabjerg, and M. Liserre,"Synchronization methods for three phase distributed power generation systems: An overview and evaluation," in *Proc. IEEE 36th Power Electronics Specialists Conf. (PESC)*, Recife, Brazil, 2005, pp. 2474–2481, doi: 10.1109/PESC.2005.1581980.

[33] P. Rodríguez, J. Pou, J. Bergas, J. I. Candela, R. P. Burgos, and D. Boroyevich,"Decoupled double synchronous reference framePLL for power converters control,"*IEEE Trans. Power Electron.*,vol. 22, no. 2, pp. 584–592, Mar. 2007,doi: 10.1109/TPEL.2006.890000.

[34] EMTP,"EMTP®: The reference for power system transients," [Online]. Available: `https://www.emtp.com/`. Accessed: Aug. 14, 2026.

A

Appendix 1

A.1 MATLAB Code For the Islanded system

This section represent the required code which is written in MATLAB to define all the parameters and variables for wind turbine model, solar model, battery model which imports the text file to MATLAB and then data is processed for further programming. The code need to be run before more simulation.

A.2 MATLAB Code

The MATLAB code used for the model is presented below.

```
clear

%========================  Inlasning av matdata
    ====================
delimiterIn = '\t';

filename1 = 'B1_CL4_20_220705_13_07_31.txt';
measurements1 = importdata(filename1, delimiterIn);

filename2 = 'B1_CL3_20_220124_11_00_44.txt';
measurements2 = importdata(filename2, delimiterIn);

filename3 = 'B1_CL4_20_220705_13_37_34.txt';
measurements3 = importdata(filename3, delimiterIn);

% If importdata returns structure, extract numeric data
if isstruct(measurements1)
    measurements1 = measurements1.data;
end

if isstruct(measurements2)
    measurements2 = measurements2.data;
end

if isstruct(measurements3)
    measurements3 = measurements3.data;
end

% Check sizes before correction
disp('Before correction:')
disp(size(measurements1))
```

```
disp(size(measurements2))
disp(size(measurements3))

% CL3 file has only 66 columns.
% Add two zero columns so it becomes 68 columns like CL4 files.
if size(measurements2,2) == 66
    measurements2(:,67:68) = zeros(size(measurements2,1),2);
end

% Check sizes after correction
disp('After correction:')
disp(size(measurements1))
disp(size(measurements2))
disp(size(measurements3))

% Now this will work
measurements = [measurements1; measurements2; measurements3];

input = measurements;

kanaluppdelning20220705;
% %========================  Inlasning av matdata
   ====================
% delimiterIn = '\t';
%
% filename1 = ['B1_CL4_20_220705_13_07_31.txt'];
% measurements1 = importdata(filename1,delimiterIn);
% filename2 = ['B1_CL3_20_220124_11_00_44.txt'];
% measurements2 = importdata(filename2,delimiterIn);
% filename3 = 'B1_CL4_20_220705_13_37_34.txt';   % change this to
   your new file name
% measurements3 = importdata(filename3, delimiterIn);
%
% measurements = [measurements1; measurements2; measurements3];
% %measurements = [measurements1; measurements2];
%
% %Inkludera foljande ifall CL3 matfil studeras:
% %measurements(:,67:68) = zeros(length(measurements(:,1)),2);
%
% input = measurements;

kanaluppdelning20220705; % Matdatan delas up i effekt,
   vindhastighet, mm.


% ==================  DC-generator komponenter:
   =====================
J           =  2600/(20^2);          % Troghetsmoment[kgm^2]
b           =  0.1;                  % Dampning
Kp          =  3;                    % PI-reg
Ki          =  5;                    % PI-reg

% ====================  NREL-reg:  ==============================
Sampl_t          = 0.05;        %  [s]          Sampling time of
   the controller
CornerFrequency  = 10;          %  [rad/s]      Corner frequency of
```

```
    the generator speed low pass filter
VS_CtInSp         = 5.7;          %  [rad/s]      Cut-in generator
   speed
VS_RtPwr          = 25000;        %  [W]          Rated generator
   power
VS_RtGnSp         = 7.45;         %  [rad/s]      Rated generator
   speed
VS_Rgn3MP         = 1.6;          %  [rad]        Pitch angle to stay
    in Region 3
VS_Slope15        = 2600;         %  [W/(rad/s)]  Slope of torque
   curve in Region 1.5
VS_Rgn2Sp         = 6.2;          %  [rad/s]      Lower generator
   speed limit for Region 2.
VS_Rgn2K          = 35;         %  [W/(rad/s)2] Region 2 generator
   torque constant.
VS_TrGnSp         = 7;         %  [rad/s]      Lower generator speed
   limit for Region 2.5.
VS_Slope25        = 3500;         %  [W/(rad/s)]  Slope of torque
   curve in Region 2.5
VS_SySp           = 6.5;          %  [rad/s]      Generator speed
   where torque would be zero if in Region 2.5. (Construction help
   point.)
VS_MaxTq          = 225;         %  [Nm]         Maximum generator
   torque
VS_MaxRat         = 500;        %  [Nm/s]       Maximum generator
   torque rate
PC_MaxPit         = 1.5708;        %  [rad]        Maximum allowed
   pitch angle (Fully feathered position)
PC_MinPit         = 0.0349;         %  [rad]        Minimum allowed
   pitch angle (Fully fine position)
PC_KP             = 0.35;         %  [rad/(rad/s)] Pitch controller
   Proportional gain
PC_KI             = 0.22;         %  [rad/(rad/s)] Pitch controller
   Integral gain
PC_KK             = 0.4;          %  [rad]        The pitch angle at
   which the pitch sensitivity is double the pitch sensitivity at
   pitch = 0 rad.
PC_MaxRat         = 0.2;          %  [rad/s]      Maximum allowed
   pitch rate
VS_SlPc           = 10;
StoppingPitchSpeed = 0.0349;      %  Pitch rate when stopping the
   turbine
StartingPitchSpeed = -0.0249;     %  [rad/s] Pitch rate when
   starting the turbine
PC_RefSpd = 7.85;                 %  [rad/s] Reference generator
   speed
Run_Stop = 1;


%=======================  Vindkraftverk parametrar
   ===================
Lambda_opt=8.75;     % Optimal lambda
rho=1.225;           % [kg/m^3] Air density
d=16;                % [m] Turbine diameter
R = d/2;             % [m] Turbine radius
Cpmax=0.418;         % Maximum Power Coefficient of the turbine with
```

```
    MinPit at 2 deg.
A=pi*R.^2;          % [m^2]Turbine area.


%=== Stopping and Starting Pitch Speed Adjustment Near Feathered
   ===
SaS =   [PC_MinPit 1;
        PC_MaxPit*0.85 1;
        PC_MaxPit*0.98 0.15;
        PC_MaxPit*1.2 0.15;];

SaS_table = SaS(1:end,2:end);
SaS_BP = SaS(1:end,1)'; % Rad index for tabell


% ======================  Cp(lambda, Beta) tabell
   =====================
load('CP_data.mat');                % Data for Cp tabell
breakpoints1 = data(2:end,1)';      % Rad index for tabell
breakpoints2 = data(1,2:end);       % Kolumn index for tabell
table_data = data(2:end,2:end);     % Output varden for tabell

% ==================== Max Cp for alla vinklar over 2 grader
   ==========
Cp_B0 = table_data;
Cp_B0(:,1) = 0;
Max_Cp = [breakpoints1' max(Cp_B0')'];
Vector_data = max(Cp_B0')';

%======================  Spill metod antal ======================
breakpoints3 = flip(table_data(32,1:7));  % Rad index for
   bladvinkel tabel
Beta = flip(breakpoints2(1:7));           %Varden for bladvinkel
Pspill = 0;                               %Antal watt som spills

%====================== Tid och effekt======================
time1=linspace(0,length(time)*Sampl_t,length(time))'; % [s]  For
   att matningarna
                          % ska borja pa t = 0
Pel=(DCV.* DCC)./1000;    % [kW] Berakna elektrisk effekt (Pel)
   med
                          % DC-link spanning (DCV) and strom (DCC)
Eleff=0.89;               % Generator varkningsgrad.
Pmec=Pel/Eleff;           % [kW] Mekanisk effekt

%============== Bearbetning av frekvens data ==================
load('FrekvensData.mat');               %Las in frekvens data
freq = Frekvens.freq_vector;            %Hamta frekvens vektor

%Leta efter position med minsta frekvens
min_freq = min(min(freq));
size_freq = size(freq);
for i = 1:size_freq(1)
    for j = 1:size_freq(2)
        if freq(i,j) == min_freq
            index=[i j];
```

```
        end
    end
end

%Skapa en 15 min lang frekvens och tid vekor runt minsta vardet
freq15 = freq(index(1),index(2)-4500:index(2)+3499);
time_freq=linspace(0,length(freq15)/10,length(freq15))'; %Div 10
   pga 10 Hz sampling av frekvens
%% ====================== Battery parameters
   ======================
% %% ====================== Battery parameters
   ======================

% Battery pack configuration
N_series   = 166;          % cells in series
N_parallel = 3;            % cells in parallel
N_cells    = N_series * N_parallel;

V_cell_min = 3.3;          % [V]
V_cell_max = 4.0;          % [V]

V_bat_min  = N_series * V_cell_min;     % [V]
V_bat_max  = N_series * V_cell_max;     % [V]
V_bat      = (V_bat_min + V_bat_max)/2; % [V] nominal/average
   voltage

% Battery energy
E_bat_kWh  = 42;                   % [kWh]
E_bat_Wh   = E_bat_kWh * 1000;     % [Wh]
E_bat      = E_bat_Wh * 3600;      % [J]

% Battery Ah capacity
C_Ah       = E_bat_Wh / V_bat;     % [Ah]
Q_bat_As   = C_Ah * 3600;          % [A.s]

% Battery power rating
P_ch_max   = 20000;                % [W] charging limit
P_dis_max  = 20000;                % [W] discharging limit

I_ch_max   = P_ch_max  / V_bat;    % [A]
I_dis_max  = P_dis_max / V_bat;    % [A]

% SOC limits
SOC_init   = 0.50;                  % 50%
SOC_min    = 0.10;                 % 10%
SOC_max    = 0.90;                 % 90%

E_bat_init = SOC_init * E_bat;
Q_bat_init = SOC_init * Q_bat_As;

% Usable battery energy
E_usable_kWh = E_bat_kWh * (SOC_max - SOC_min);

% fprintf('Battery voltage range: %.1f - %.1f V\n', V_bat_min,
   V_bat_max);
% fprintf('Nominal battery voltage: %.1f V\n', V_bat);
```

```
% fprintf('Battery capacity: %.1f Ah\n', C_Ah);
% fprintf('Usable battery energy: %.1f kWh\n', E_usable_kWh);
% fprintf('Max charge/discharge current: %.1f A / %.1f A\n',
    I_ch_max, I_dis_max);
%
    %%%%%%%%%%%%%%%%%%%%%%%%%%%%%%%%%%%%%%%%%%%%%%%%%%%%%%%%%%%%%%%%%%%%

% P_ch_max   = 5000;                 % [W]
% P_dis_max  = 5000;                 % [W]
% V_bat      = 500;                  % [V]
% E_bat_kWh  = 20;                   % [kWh]
% E_bat_Wh   = E_bat_kWh * 1000;     % [Wh]
% E_bat      = E_bat_Wh * 3600;      % [J]
% C_Ah       = E_bat_Wh / V_bat;     % [Ah]
% Q_bat_As   = C_Ah * 3600;          % [A s]
%
% SOC_init   = 0.5;
% SOC_min    = 0.1;
% SOC_max    = 0.9;
%
% E_bat_init = SOC_init * E_bat;
% Q_bat_init = SOC_init * Q_bat_As;
% I_ch_max   = P_ch_max  / V_bat;
% I_dis_max  = P_dis_max / V_bat;
%% ============================================================
% PV MODEL INITIALIZATION FOR ~1500 W ARRAY
% Cell-based model + Ns/Np scaling
%
% Assumption:
% - Base module: 250 W class module
% - 60 cells/module
% - 6 modules in series
% - 1 parallel string
%
% Notes:
% - I corrected V_cell and Voc_module so the array stays near 1500
    W.
%% ============================================================

% Time base for solar uses same time as wind script
t = time1;

% PV operating point near MPP
V_cell = 0.55;                  % [V] corrected from 1.4 to 0.5

% Temperature
T_pv   = 25;                   % [degC]
T_ref  = 25;                   % [degC]

% Photocurrent parameters
Isc = 9.9;                     % [A]
Ksc = 0.005;                   % [A/degC]

% Physical constants
q = 1.602e-19;                 % [C]
k = 1.381e-23;                 % [J/K]
```

```
T_kelvin = T_pv + 273.15;      % [K]
Vt = k*T_kelvin/q;             % [V]

% Diode ideality factor
alpha = 1.3;

% Open-circuit voltage
Voc_module = 120;              % [V] corrected from 148 to 37
Voc_cell   = Voc_module / 60; % [V]

% Diode saturation current
Io = Isc / (exp(Voc_cell/(alpha*Vt)) - 1);

% Resistance parameters
Rs  = 0.005;                   % [ohm]
Rsh = 200;                     % [ohm]

% Array scaling
Ns_mod            = 6;         % series modules
cells_per_module  = 60;
Ns                = Ns_mod * cells_per_module;   % 360 series cells
Np                = 8;

% Synthetic irradiance profile aligned to full simulation length
%
   %%%%%%%%%%%%%%%%%%%%%%%%%%%%%%%%%%%%%%%%%%%%%%%%%%%%%%%%%%%%%%%%%%%%%%%%%%%%%%

% %% ================= Realistic solar irradiance data for 1800 s
   =================

%% ================= Read solar irradiance from Excel file for 1800
    s =================

% Excel file generated from 24-hour irradiance compressed to 1800 s
filename1 = 'Irradiance_1800_from_24hr.xlsx';

% Read Excel file
% Expected columns:
% Column 1 = Time_sec
% Column 2 = Solar_Irradiance_W_per_m2
input1 = readmatrix(filename1);

% Remove empty rows if any
input1 = input1(~all(isnan(input1), 2), :);

% Extract time and irradiance
t = input1(:,1);         % [s]
G_data = input1(:,2);    % [W/m^2]

% Clean data
G_data = fillmissing(G_data, 'linear', 'EndValues', 'nearest');
G_data(G_data < 0) = 0;

% Make sure time starts from zero
t = t - t(1);
```

```
% Convert to Simulink timetable input
G = timetable(seconds(t), G_data);

% Plot to check
figure;
plot(t, G_data, 'LineWidth', 1.5);
xlabel('Time␣[s]');
ylabel('Solar␣Irradiance␣[W/m^2]');
title('Solar␣Irradiance␣Input␣from␣Excel␣File');
grid on;

disp('Solar␣irradiance␣Excel␣file␣loaded␣successfully.');
disp('Timetable␣variable␣G␣is␣ready␣for␣Simulink.');

%
   %%%%%%%%%%%%%%%%%%%%%%%%%%%%%%%%%%%%%%%%%%%%%%%%%%%%%%%%%%%%%%%%%%%%%%%%%%%%%%%%%%%%%%%%%%%%%%%%%%%%%%%%

%
%
% % Time vector
% t = (0:1:1800)';          % [s], 1 second sample time
%
% % Normalized time
% tau = t / t(end);
%
% % Base irradiance shape
% % Starts low, increases, reaches high value, then slightly
   decreases
% G_clear = 150 + 850 * sin(pi * tau).^0.75;
%
% % Add realistic cloud dips using Gaussian-shaped reductions
% cloud1 = 350 * exp(-((t - 420)/90).^2);      % cloud around 420 s
% cloud2 = 500 * exp(-((t - 950)/120).^2);     % stronger cloud
   around 950 s
% cloud3 = 300 * exp(-((t - 1380)/100).^2);    % cloud around 1380 s
%
% % Small fast fluctuations caused by passing clouds / sensor
   variation
% rng(1);   % keeps same random profile every time
% noise = 25 * randn(size(t));
%
% % Final irradiance
% G_data = G_clear - cloud1 - cloud2 - cloud3 + noise;
%
% % Limit irradiance between realistic minimum and maximum values
% G_data = max(G_data, 0);
% G_data = min(G_data, 1000);
%
% % Smooth slightly to avoid unrealistic sharp noise
% G_data = smoothdata(G_data, 'movmean', 15);
%
% % Convert to Simulink timetable input
% G = timetable(seconds(t), G_data);
%
% % Plot
% figure;
```

```
% plot(t, G_data, 'LineWidth', 1.5);
% xlabel('Time [s]');
% ylabel('Solar Irradiance [W/m^2]');
% title('Realistic Solar Irradiance Profile for 1800 Seconds');
% grid on;
%
    %%%%%%%%%%%%%%%%%%%%%%%%%%%%%%%%%%%%%%%%%%%%%%%%%%%%%%%%%%%%%%%%

% G_data = zeros(size(t));
% tau = t / max(t(end), eps);
%
% for k_idx = 1:length(t)
%     if tau(k_idx) < 0.20
%         G_data(k_idx) = 200;
%     elseif tau(k_idx) < 0.50
%         G_data(k_idx) = 1000;
%     elseif tau(k_idx) < 0.70
%         G_data(k_idx) = 400;
%     else
%         G_data(k_idx) = 800;
%     end
% end

% Optional irradiance signal for Simulink From Workspace / root
    inport
G_signal = timeseries(G_data, t);

% --------- Cell current from single-diode equation (fixed-point)
    ---------
Iph = (Isc + Ksc*(T_pv - T_ref)) .* (G_data/1000);   % [A]
I_cell = Iph;

for it = 1:50
    arg = (V_cell + I_cell.*Rs) ./ (alpha*Vt);
    arg = min(arg, 80); % numerical protection
    I_new = Iph - Io.*(exp(arg) - 1) - (V_cell + I_cell.*Rs)./Rsh;
    I_cell = max(I_new, 0);
end

V_array_est = Ns * V_cell;    % [V]
I_array_est = Np * I_cell;    % [A]
P_solar_profile = V_array_est .* I_array_est;
P_solar_profile = max(P_solar_profile, 0);

% Optional hard cap near array rating
P_solar_rated = 1500;                        % [W]
P_solar_profile = min(P_solar_profile, P_solar_rated);

% ============= Input till Simulink =====================

% Generator hastighet
GenSpeed = timetable(seconds(time1),TurbSpeed2);

% Vind hastighet
Wind = timetable(seconds(time1), WS30);
```

```
% Spets hastighet
V_tip = timetable(seconds(time1), (2*pi*TurbSpeed2)/60*R);

% Elektrisk effekt
P_mec = timetable(seconds(time1), Pmec*1000);

% Mekanisk effekt
P_el = timetable(seconds(time1), Pel*1000);

% Bladvinkel grader
Vinkel = timetable(seconds(time1), PAB1);

% Tillganglig effekt fran vindkraftverk
MPE = timetable(seconds(time1), MaxPwrEst);

% Frekvens data
Frekvens = timetable(seconds(time_freq), freq15');

%FFR signal
FFR_sig = timetable(seconds(time1), Marker);

%P_Wasted
P_waste = timetable(seconds(time1), Pwaste);

% Nat frekvens
Fgrid = timetable(seconds(time1), Fgrid);

%================== Hamta parametrar fran modell ===============
out = sim('wind_turbine_model');
open('wind_turbine_model');

time_out = get(out,"tout");                        %Hamta tid vektor
Bladvinkel = get(out, 'Bladvinkel');               %Hamta uppmatt
    bladvinkel
Bladvinkel_sim = get(out, 'Bladvinkel_sim');       %Hamta simulerad
    baldvinkel
Varvtal = get(out, 'Vinkelhastighet');             %Hamta uppmatt
    varvtal
Varvtal_sim = get(out, 'Vinkelhastighet_sim');     %Hamta simulerat
    varvtal
Effekt = get(out, 'Effekt');                       %Hamta uppmatt
    effekt
Effekt_sim = get(out, 'Effekt_sim');               %Hamta simulerad
    effekt
Tillganglig = get(out, "Tillganglig");

%================== Passning av modell ======================
remove_t = 90*(1/Sampl_t);  %Ta bort de forsta 90 sekunder for att
    undvika upprampning av modellen
time_out(1:remove_t) = [];
Varvtal(1:remove_t) = [];
Bladvinkel(1:remove_t) = [];
Effekt(1:remove_t) = [];
Varvtal_sim(1:remove_t) = [];
Bladvinkel_sim(1:remove_t) = [];
Effekt_sim(1:remove_t) = [];
```

```
Tillganglig(1:remove_t) = [];

y_bar(1) = max(Varvtal)-min(Varvtal);
y_bar(2) = max(Bladvinkel)-min(Bladvinkel);
y_bar(3) = max(Effekt)-min(Effekt);

%Chi 2
Chi2(1) = 1./length(Varvtal)*sum((Varvtal-Varvtal_sim).^2./
   Varvtal_sim);                    %berakna chi^2 for varvtal
Chi2(2) = 1./length(Bladvinkel)*sum((Bladvinkel-Bladvinkel_sim)
   .^2./Bladvinkel_sim);        %berakna chi^2 for bladvinkel
Chi2(3) = 1./length(Effekt)*sum((Effekt-Effekt_sim).^2./Effekt_sim)
   ;
Chi2(4) = 1./length(Effekt)*sum((Effekt-Tillganglig).^2./
   Tillganglig)                           %berakna chi^2 for effekt

%MAE
MAE(1) = 1./length(Varvtal)*sum(abs(Varvtal-Varvtal_sim));
                     %berakna chi^2 for varvtal
MAE(2) = 1./length(Bladvinkel)*sum(abs(Bladvinkel-Bladvinkel_sim));
           %berakna chi^2 for bladvinkel
MAE(3) = 1./length(Effekt)*sum(abs(Effekt-Effekt_sim));
                        %berakna chi^2 for effekt
MAE(4) = 1./length(Effekt)*sum(abs(Effekt-Tillganglig))

%NMAE
NMAE(1) = 1./(length(Varvtal)*y_bar(1))*sum(abs(Varvtal-Varvtal_sim
   ));                      %berakna chi^2 for varvtal
NMAE(2) = 1./(length(Bladvinkel)*y_bar(2))*sum(abs(Bladvinkel-
   Bladvinkel_sim));         %berakna chi^2 for bladvinkel
NMAE(3) = 1./(length(Effekt)*y_bar(3))*sum(abs(Effekt-Effekt_sim));
                        %berakna chi^2 for effekt
NMAE(4) = 1./(length(Effekt)*y_bar(3))*sum(abs(Effekt-Tillganglig))

%NRMSE
NRMSE(1) = 1/y_bar(1)*sqrt(sum((Varvtal-Varvtal_sim).^2)/length(
   Varvtal));                       %berakna chi^2 for varvtal
NRMSE(2) = 1/y_bar(2)*sqrt(sum((Bladvinkel-Bladvinkel_sim).^2)/
   length(Bladvinkel));         %berakna chi^2 for bladvinkel
NRMSE(3) = 1/y_bar(3)*sqrt(sum((Effekt-Effekt_sim).^2)/length(
   Effekt));                        %berakna chi^2 for effekt
NRMSE(4) = 1/y_bar(3)*sqrt(sum((Effekt-Tillganglig).^2)/length(
   Effekt))

%==================== pitchaktivitet ================

aktivitet=[0; abs(diff(Bladvinkel))];       %lagger till 0 for att
   aktivitet skall ha samma langd som tid
medelaktivitet=sum(aktivitet) / (time_out(end)-time_out(1))    %
   medelvarde av grader / sekund for uppmatt signal

aktivitet_sim=[0; abs(diff(Bladvinkel_sim))];
medelaktivitet_sim=sum(aktivitet_sim) / (time_out(end)-time_out(1))
     % medelvarde av grader / sekund for simulerad signal
```

A.3 MATLAB Code used For the power balance controller

The MATLAB code used for power balance logic below.

```
function [P_batt_ref, P_pv_curt, P_wind_curt, P_load_shed] =
   ems_controller(P_load, P_wind, P_solar, SOC)
% EMS controller for islanded wind-solar-battery system
%
% Inputs:
%   P_load   : load demand [W]
%   P_wind   : available wind power [W]
%   P_solar  : available solar power [W]
%   SOC      : battery state of charge [%]
%
% Outputs:
%   P_batt_ref  : battery power reference [W]
%                 +ve = discharge, -ve = charge
%   P_pv_curt   : curtailed PV power [W]
%   P_wind_curt : curtailed wind power [W]
%   P_load_shed : load to be shed [W]

% Total renewable power
P_ren = P_wind + P_solar;

% Initialize outputs
P_batt_ref  = 0;
P_pv_curt   = 0;
P_wind_curt = 0;
P_load_shed = 0;

% ============================================================
% CONDITION 1:
% P_ren > P_load and SOC < 90%
% Charge battery with surplus
% ============================================================
if (P_ren > P_load) && (SOC < 90)

    surplus = P_ren - P_load;

    % Battery charges with surplus
    P_batt_ref = -surplus;   % negative = charging

    % No curtailment, no shedding
    P_pv_curt   = 0;
    P_wind_curt = 0;
    P_load_shed = 0;

% ============================================================
% CONDITION 3:
% P_ren > P_load and SOC >= 90%
% Curtail PV first, then wind
% Battery does not charge further
% ============================================================
elseif (P_ren > P_load) && (SOC >= 90)
```

```
    surplus = P_ren - P_load;

    % Curtail PV first
    P_pv_curt = min(P_solar, surplus);

    % Remaining surplus
    rem_surplus = surplus - P_pv_curt;

    % Curtail wind next
    P_wind_curt = min(P_wind, rem_surplus);

    % Battery idle
    P_batt_ref = 0;

    % No load shedding
    P_load_shed = 0;

% ============================================================
% DEFICIT CASE:
% P_ren < P_load
% ============================================================
elseif (P_ren < P_load)

    deficit = P_load - P_ren;

    % ------------------------------------------------------
    % CONDITION 4:
    % SOC <= 25%
    % Protect battery and shed load
    % ------------------------------------------------------
    if (SOC <= 25)

        P_batt_ref = 0;
        P_pv_curt = 0;
        P_wind_curt = 0;

        % Since battery is protected, unmet demand is shed
        P_load_shed = deficit;

    % ------------------------------------------------------
    % CONDITION 2:
    % SOC > 25%
    % Battery discharges to cover deficit
    % ------------------------------------------------------
    else

        P_batt_ref = deficit;   % positive = discharge
        P_pv_curt = 0;
        P_wind_curt = 0;
        P_load_shed = 0;

    end

% ============================================================
% BALANCED CASE:
```

```
% P_ren == P_load
% ============================================================
else

    P_batt_ref = 0;
    P_pv_curt = 0;
    P_wind_curt = 0;
    P_load_shed = 0;

end
```

DEPARTMENT OF ELECTRICAL ENGINEERING
CHALMERS UNIVERSITY OF TECHNOLOGY
Gothenburg, Sweden
www.chalmers.se



CHALMERS
UNIVERSITY OF TECHNOLOGY